

1 **Impact of fossil and non-fossil sources on the molecular compositions of water soluble humic-**
2 **like substance in PM_{2.5} at a suburb site of Yangtze River Delta, China**

3
4 Mengying Bao^{1,2,3}, Yan-Lin Zhang^{1,2,*}, Fang Cao^{1,2}, Yihang Hong^{1,2}, Yu-Chi Lin^{1,2}, Mingyuan Yu^{1,2},
5 Hongxing Jiang^{4,5}, Zhineng Cheng^{4,5}, Rongshuang Xu^{1,2}, Xiaoying Yang^{1,2}

6
7 *1 School of Applied Meteorology, Nanjing University of Information Science & Technology,*
8 *Nanjing 210044, China.*

9 *2 Atmospheric Environment Center, Joint Laboratory for International Cooperation on Climate*
10 *and Environmental Change, Ministry of Education (ILCEC), Nanjing University of Information*
11 *Science & Technology, Nanjing 210044, China.*

12 *3 Huzhou Meteorological Administration, Huzhou 313300, China*

13 *4 State Key Laboratory of Organic Geochemistry and Guangdong province Key Laboratory of*
14 *Environmental Protection and Resources Utilization, Guangzhou Institute of Geochemistry,*
15 *Chinese Academy of Sciences, Guangzhou 510640, China.*

16 *5 CAS Center for Excellence in Deep Earth Science, Guangzhou 510640, China*

17 *Correspondence: Yan-Lin Zhang (dryanlinzhang@outlook.com)*

18

19 **Abstract**

20 Atmospheric humic-like substances (HULIS) affect global radiation balance due to their
21 strong light absorption at the ultraviolet wavelength. The potential sources and molecular
22 compositions of water soluble HULIS at a suburb site of Yangtze River Delta from 2017 to 2018
23 were discussed based on the radiocarbon (¹⁴C) analysis combining the Fourier Transform Ion
24 Cyclotron Resonance Mass Spectrometry (FT-ICR MS) technique in this study. The ¹⁴C results
25 showed that the averaged non-fossil source contributions to HULIS were 39 ± 8 % and 36 ± 6 %
26 in summer and winter, respectively, indicating the significant contributions from fossil sources to
27 HULIS. The Van Krevelen diagrams obtained from the FT-ICR MS results showed that the
28 proportions of tannins-like and carbohydrates-like groups were higher in summer, suggesting
29 significant contribution of HULIS from biogenic secondary organic aerosols (SOA). The higher
30 proportions of condensed aromatic structures in winter suggested increasing anthropogenic
31 emissions. Molecular composition analysis on the CHO, CHON, CHOS, and CHONS subgroups

32 showed the relatively higher intensities of high O-containing macromolecular oligomers in CHO
33 compounds in summer, further indicating stronger biogenic SOA formation in summer. High-
34 intensity phenolic substances and flavonoids which were related to biomass burning and polycyclic
35 aromatic hydrocarbons (PAHs) derivatives indicating fossil fuel combustion emissions were found
36 in winter CHO compounds. Besides, two high-intensity CHO compounds containing condensed
37 aromatic ring structures ($C_9H_6O_7$ and $C_{10}H_5O_8$) identified in summer and winter samples were
38 similar to those from off-road engine samples, indicating that traffic emission was one of the
39 important fossil sources of HULIS at the study site. The CHON compounds were mainly composed
40 of nitro compounds or organonitrates with significantly higher intensities in winter, which was
41 associated to biomass burning emission, as well as the enhanced formation of organonitrates due
42 to high NO_x in winter. However, the high-intensity CHON molecular formulas in summer were
43 referring to N-heterocyclic aromatic compounds, which were produced from the atmospheric
44 secondary processes involving reduced N species (e.g., ammonium). The S-containing compounds
45 were mainly composed of organosulfates (OSs) derived from biogenic precursors, long-chain
46 alkane and aromatic hydrocarbon, illustrating the mixed sources of HULIS. Generally, different
47 policies need to be considered for each season due to the different season sources, i.e., biogenic
48 emission in summer and biomass burning in winter for non-fossil source, traffic emission and
49 anthropogenic SOA formation in both seasons and additional coal combustion in winter. Measures
50 to control emissions from motor vehicles and industrial processes need to be considered in summer.
51 Additional control measures on coal power plants and biomass burning should be concerned in
52 winter. These findings add to our understanding of the interaction between the sources and the
53 molecular compositions of atmospheric HULIS.

54

55 **1. Introduction**

56 Atmospheric humic-like substances (HULIS) have been observed worldwide and can be
57 produced from primary combustion of biomass, fossil fuel, as well as various secondary processes
58 such as photochemical processes of volatile organic compounds (VOCs) and heterogeneous
59 reactions of organic aerosols in the atmosphere (Kuang et al., 2015; Li et al., 2019; Ma et al., 2018;
60 Sun et al., 2021). As important component of brown carbon (BrC) aerosols, HULIS species have
61 been widely reported to have a great impact on global radiative budget, contributing to 20-40% of
62 the direct radiative forcing caused by light absorbing aerosols due to its light absorption at the

63 ultraviolet wavelength (Chung et al., 2012; Zhang et al., 2017; Zhang et al., 2020a; Wang et al.,
64 2018c). HULIS are a highly complex mixture of polar organic compounds composed of aromatic
65 and hydrophobic aliphatic structures containing carboxyl, carbonyl, and hydroxyl function groups
66 (Zheng et al., 2013; Graber and Rudich, 2006; Zhang et al., 2022b; Zhang et al., 2022c). During
67 the atmospheric secondary oxidation processes, the substitutions of hydrophilic functional groups
68 increased aerosol hygroscopicity (Huo et al., 2021; Jiang et al., 2020). Polycarboxylic acids in
69 HULIS are surface-active and play an important role in the cloud condensation nuclei (CCN)
70 activity (Tsui and McNeill, 2018). N-base compounds can promote the generation of atmospheric
71 reactive oxygen species (ROS) which have a great impact on human health (Wang et al., 2017c;
72 De Haan et al., 2018; Song et al., 2022). Identifying the molecular compositions of HULIS is a
73 challenge due to complex mixtures contained in HULIS and can help to a better understanding of
74 the processes involving organic compounds in atmosphere (Noziere et al., 2015; Laskin et al.,
75 2018).

76 The Fourier-Transform Ion Cyclotron Resonance Mass Spectrometry (FT-ICR MS) coupled
77 with electrospray ionization (ESI) ion source have been widely used in identifying the chemical
78 structure of HULIS, providing high mass accuracy and can determine molecular formulas from
79 mixed compounds (Chen et al., 2016; Wang et al., 2019b; Lin et al., 2012a; Jiang et al., 2020).
80 Typical molecular formulas composed of C, H, and O atoms in HULIS were observed being
81 abundant in carboxylic acids, lignin-derived products, and polycyclic aromatic hydrocarbons
82 (PAHs) or their derivatives (Lin et al., 2012a; Sun et al., 2021; Jiang et al., 2020; Huo et al., 2021;
83 Song et al., 2018). In addition, the HULIS formation of N and S containing precursors was also
84 widely detected. The N-containing compounds such as nitroaromatics were important
85 chromophores in HULIS in aged biomass burning organic aerosols (BBOA), as well as in ambient
86 aerosols influenced by biomass burning (BB), while reduced N compounds such as N-heterocyclic
87 aromatic compounds were found to be important chromophores in fresh BBOA (Wang et al.,
88 2019b; Song et al., 2022; Jiang et al., 2020; Wang et al., 2017c). Recent laboratory simulation
89 experiments showed that the photooxidation of various anthropogenic VOCs (e.g., naphthalene,
90 benzene, toluene, and ethylbenzene) would be promoted under high NO_x condition, producing
91 strongly light absorbing nitroaromatics (Yang et al., 2022; Aiona et al., 2018; Siemens et al., 2022;
92 Xie et al., 2017). Otherwise, nighttime oxidation of biogenic or anthropogenic VOCs, such as
93 benzene/toluene, isoprene (C₅H₈) and monoterpenes (C₁₀H₁₆) by NO₃ radicals lead to substantial

94 organonitrates formation, where the VOCs oxidation is strongly affected by NO_x (He et al., 2021;
95 Shen et al., 2021; Wang et al., 2020; Zheng et al., 2021).

96 The organosulfates (OSs) and nitrooxy organosulfates (nitrooxy-OSs) have also been found
97 to widely exist in HULIS in different atmospheric environment (Lin et al., 2012b; Lin et al., 2012a;
98 Sun et al., 2021). Field study and laboratory smog chamber experiments have confirmed that OSs
99 and nitrooxy-OSs in the atmosphere mainly come from the O₃, OH, or NO₃ oxidation of biogenic
100 VOCs such as isoprene, α/β-pinene as well as aromatic hydrocarbon in the presence of H₂SO₄/SO₂
101 (Surratt et al., 2008; Glasius et al., 2021; Yang et al., 2020; Lin et al., 2012b; Huang et al., 2020).
102 Coal combustions were found to be important sources of the aromatic OSs and nitrooxy-OSs in
103 HULIS (Song et al., 2018). Besides, the long-chain alkanes were found to be important precursor
104 of OSs in atmospheric aerosol samples from urban area which was related to vehicle emissions
105 (Wang et al., 2019a; Tao et al., 2014).

106 Nanjing is one of the main cities in the Yangtze River Delta (YRD), which is one of the most
107 developed areas in China. Organic matter can account for 20-40 % of PM_{2.5} in the YRD area due
108 to the impact of complicated sources, especially anthropogenic emissions (Wang et al., 2017a;
109 Wang et al., 2016a). Studies have reported that BrC is an important contributor to aerosol light
110 absorption in Nanjing and exhibited obvious seasonal variations, with peaks in wintertime, owing
111 to emissions from biomass burning, fossil fuel combustion, and secondary formation (Chen et al.,
112 2018; Cui et al., 2021; Xie et al., 2020; Wang et al., 2018a). Recently, works on the field
113 observation of nitrated aromatic compounds (NACs) were conducted to explore the light
114 absorption contributions of NACs to BrC and help to better understand the links between the
115 optical properties and molecular compositions of BrC (Gu et al., 2022; Cao et al., 2023). However,
116 as far as we know, understanding of the sources of atmospheric HULIS at molecular levels was
117 still limited. In this work, the molecular compositions of water soluble HULIS isolated from PM_{2.5}
118 samples collected in summertime and wintertime from 2017 to 2018 at Nanjing, China, were
119 investigated combining the FT-ICR MS and radiocarbon (¹⁴C) analysis. We aim to obtain the
120 molecular characteristic differences of water soluble HULIS in summertime and wintertime and
121 to get a better understanding of the influence of different sources on the molecular compositions
122 of HULIS.

123 **2. Materials and methods**

124 **2.1 Sample collection**

125 The 24 h PM_{2.5} samples were collected on the roof of Wende building, which was about 21
126 m height from the ground at Nanjing University of Information Science and Technology (32.2° N,
127 118.7° E) using a high-volume sampler (KC-1000, Qingdao, China) at a flow rate of 300 L min⁻¹.
128 The study site was located in the northern suburb area of Nanjing, adjacent to G205 State Road
129 and surrounded by an industrial park and residential area. Generally, the study site was affected
130 by human activity, industrial emission, and traffic emission. The sample collection was conducted
131 in summer from 12 August 2017 to 26 August 2017 and in winter from 31 December 2017 to 31
132 January 2018. A heavy haze event occurred from 31 December 2017 to 3 January 2018, thus the
133 sample frequency was adjusted to 2 h in daytime and 8 h in nighttime. Field blank filters were
134 performed before and after sample collection for each season. More details about the sample
135 collection can be found in previous research reported by Bao et al. (2022). The air pollutants data
136 including PM_{2.5}, SO₂ and NO₂ were provided by China National Environmental Monitoring Centre.
137 Twelve samples were selected for further chemical analysis and the details about the sample
138 selection are described in Section 3.1 in this study.

139 2.2 Chemical analysis

140 The solid phase extraction (SPE) cartridge (Oasis HLB, 30 μm, 60 mg/cartridge, Waters,
141 USA) was performed to isolate the water soluble HULIS in this study. Briefly, the prepared water
142 extracts passed through the pre-conditioned HLB cartridge firstly, then the retained HULIS on the
143 HLB cartridge were eluted with 2% (v/v) ammonia/methanol and evaporated to dryness under a
144 gentle stream of nitrogen gas, then re-dissolved in ultrapure water for the measurement. The carbon
145 fraction in HULIS (HULIS-C) were determined using a total carbon analyzer (Shimadzu-TOC-
146 VCPH, Shimadzu, Japan) with standard deviation of reproducibility test less than 3.5 % and
147 detection limit of 0.14 μg C m⁻³. More details about the HULIS isolation and measurement have
148 been described in Bao et al. (2022).

149 The mass concentrations of the water soluble ions including NO₃⁻, NH₄⁺ and SO₄²⁻ were
150 measured using an ion chromatography (Dionex ICS-5000+, ThermoFisher Scientific, USA)
151 separated on an AS11 column (4*250 mm, Dionex). Potassium hydrate (KOH) was used as the
152 gradient eluent for anion determination. The levoglucosan concentrations were analyzed using the
153 same ion chromatograph equipped with a CarboPac MA1 analytical column (4*250 mm, Dionex)
154 and an electrochemical detector. Sodium hydroxide (NaOH) was used as the gradient eluent for

155 levoglucosan determination. All data were blank corrected in this study. More details of the
156 methods have been described previously (Liu et al., 2019).

157 2.3 Radiocarbon analysis

158 For the radiocarbon measurement of the HULIS samples, the organic solvents were firstly
159 evaporated under a gentle flow of ultrapure N₂ for 30-40 minutes in tin cups. After that, the tin
160 cups were wrapped into balls and more than 50 µg of carbon from the HULIS samples was
161 combusted into CO₂ using an elemental analyzer (EA, model vario micro, elemental, Germany),
162 then reduced into graphite targets for ¹⁴C determination at the State Key Laboratory of Organic
163 Geochemistry, Guangzhou Institute of Geochemistry, Guangzhou, China (Jiang et al., 2020).
164 Detailed descriptions of the ¹⁴C data processing can be found in previous study (Mo et al., 2018).
165 Briefly, the ¹⁴C values were expressed as the modern carbon (f_m) fraction after correcting for the
166 $\delta^{13}\text{C}$ fractionation. The f_m was converted into non-fossil carbon (f_{nf}) fraction with the correction
167 factor of 1.06 ± 0.07 based on the long-term time series of ¹⁴CO₂ sampled at the background station
168 in this study (Levin et al., 2013; Levin and Kromer, 2004). ¹⁴C analysis of the oxalic acid standard
169 (IAEA-C7) was conducted in this study (Xu et al., 2021). No field blank correction was performed
170 for the carbon isotope analysis since the carbon content in the field blanks was negligible.

171 2.4 High-resolution FT-ICR MS analysis

172 The ultrahigh resolution mass spectra of the HULIS samples were obtained through a Solarix
173 XR FT-ICR MS (Bruker Daltonics, GmbH, Bremen, Germany) equipped with a 9.4 T
174 superconducting magnet (Gamry Instruments, Warminster, USA) and a Paracell analyzer cell
175 (Bruker Daltonik GmbH, Bremen, Germany) in the negative ESI mode. The detection mass range
176 was set as m/z 150 to 800 and the ion accumulation time was set as 0.65 s. A total of 100 continuous
177 4M transient data points were superposed to enhance the signal to noise ratio and dynamic range.
178 The mass spectrum was externally calibrated with a standard solution of arginine and internal
179 recalibration was performed using typical O₆S₁ chemical species in DataAnalysis ver. 4.4 software
180 (Bruker Daltonics) (Mo et al., 2018; Tang et al., 2020; Jiang et al., 2020). Field blank filters were
181 analyzed as same as the samples and all the sample data were blank corrected. More details about
182 the data processing can be found in Text S1 in the supporting information.

183 3. Results and discussion

184 3.1 General temporal characteristics during the sampling periods

185 Figure 1 displays the temporal variations of non-fossil contributions to HULIS-C, the mass
186 concentrations of HULIS-C, levoglucosan, NO_3^- , SO_4^{2-} , NH_4^+ , SO_2 , NO_2 , and $\text{PM}_{2.5}$, as well as the
187 relative humidity and temperature during the study periods corresponding to the 12 samples. The
188 12 samples were named as S1-S6 (summer) and W1-W6 (winter) in chronological order
189 corresponding to the six samples in summer and winter, respectively in this study. The averaged
190 mass concentrations of $\text{PM}_{2.5}$ in summer and winter during the selected periods were 21.05 ± 8.05
191 $\mu\text{g m}^{-3}$ and $445.67 \pm 275.00 \mu\text{g m}^{-3}$, respectively, indicating the serious pollution level in winter.
192 The daily $\text{PM}_{2.5}$ mass concentrations in summer were all below the daily averaged Chinese
193 National Ambient Air Quality Standard (NAAQS) of $35 \mu\text{g m}^{-3}$, while the daily $\text{PM}_{2.5}$ mass
194 concentrations in winter all exceeded the daily averaged NAAQS of $35 \mu\text{g m}^{-3}$, of which the $\text{PM}_{2.5}$
195 mass concentrations of W1-W3 and W6 exceeded $200 \mu\text{g m}^{-3}$. The averaged mass concentrations
196 of HULIS in summer and winter during the selected periods were $1.83 \pm 0.27 \mu\text{g m}^{-3}$ and $4.52 \pm$
197 $2.29 \mu\text{g m}^{-3}$, respectively. The averaged HULIS concentration in summer was comparable with
198 those measured in other cities in China, i.e., $1.70 \mu\text{g m}^{-3}$ in Guangzhou, $1.61 \mu\text{g m}^{-3}$ in Shanghai
199 and $1.50 \mu\text{g m}^{-3}$ in Xi'an. Compared with those measured in winter samples in other cities, our
200 result was comparable with those in Xi'an ($4.50 \mu\text{g m}^{-3}$), a little lower than those in the megacity
201 of Shanghai ($5.31 \mu\text{g m}^{-3}$) and higher than those in the southern coastal city of Guangzhou ($3.6 \mu\text{g}$
202 m^{-3}) (Fan et al., 2016; Zhang et al., 2020b; Zhao et al., 2016).

203 As shown in Fig. 1, the mass concentrations of HULIS-C, levoglucosan, water soluble
204 secondary inorganic aerosols (SIA), and air pollutants showed similar trends in winter, suggesting
205 the influence of BB and anthropogenic emissions in winter (Wu et al., 2019b). The radiocarbon
206 analysis results showed that the f_{nf} of HULIS-C ranged from 30 % to 50 % with an average
207 contribution of 39 ± 8 % in summer and ranged from 32 % to 48 % with an average contribution
208 of 36 ± 6 % in winter, indicating the significant contributions from fossil sources to HULIS at the
209 study site. The 48 h back trajectories (Fig. S1) showed that the study site was affected by the
210 polluted air masses mainly from the northern cities in winter, suggesting the coal combustion
211 contributions to HULIS in winter (Ma et al., 2018; Sun et al., 2021). In addition, significant
212 increasing of the levoglucosan and HULIS-C mass concentrations were found from 31 December
213 2017 to 1 January 2018, corresponding to the W1-W3 samples and the maximum of the
214 levoglucosan and HULIS-C mass concentrations were 552.79 ng m^{-3} and $7.40 \mu\text{g m}^{-3}$, respectively,
215 indicating the BB impact during the periods. In summer, the study site was affected by both

216 regional transport from the nearby cities in the north and west of Nanjing and the Donghai Sea.
217 The anthropogenic emissions from the neighboring cities might cause the anthropogenic SOA
218 formation, i.e., secondary N-containing and S-containing compounds with aromatic structures
219 during the atmospheric transport processes, which was discussed in detail in section 3.4 in this
220 study.

221 3.2 Mass spectra and molecular formula assignments

222 Figure S2 and S3 show the negative ion ESI FT-ICR mass spectra of HULIS in summer and
223 winter, respectively. The molecular formulas listed are some of the top ten molecular formulas.
224 Thousands of peaks are present in the spectra in the range from m/z 150 to m/z 600 and the most
225 intense ion peaks are those in the range m/z 200-400 in summer and m/z 150-350 in winter. Our
226 results are similar to those found for the ultrahigh resolution mass spectra of water-soluble organic
227 compounds in particles produced from BB, coal combustion, vehicle exhaust emissions, as well as
228 in ambient aerosols and cloud water samples, within a reasonable range (Tang et al., 2020; Sun et
229 al., 2021; Song et al., 2018; Song et al., 2019; Bianco et al., 2018). In this study, the assigned
230 molecular formulas were classified into the following four main subgroups based on their
231 elemental compositions: CHO (compounds containing only C, H, and O), CHON (compounds
232 containing C, H, O and N), CHOS (compounds containing C, H, O, and S), and CHONS
233 (compounds containing C, H, O, N, and S). As shown in Fig. 2, the proportions of the four
234 subgroups accounted for the overall formulas followed as CHO (20 %-27 %), CHON (28 %-43 %),
235 CHOS (19 %-26 %), and CHONS (16 %-26 %) in summer, respectively and CHO (15 %-19 %),
236 CHON (30 %-40 %), CHOS (21 %-32 %), and CHONS (20 %-29 %) in winter, respectively. The
237 average proportions of the CHO, CHON, CHOS, and CHONS compounds in summer were $22 \pm$
238 3% , $36 \pm 5 \%$, $22 \pm 3 \%$, and $20 \pm 4 \%$, respectively. The average proportions of the four subgroups
239 in winter were $17 \pm 2 \%$, $32 \pm 4 \%$, $24 \pm 3 \%$, and $27 \pm 4 \%$, respectively. The CHON groups were
240 the major components of molecular formulas, furthermore, the relative intensity of CHON groups
241 increased significantly in winter (Fig. S2 and Fig. S3). Studies have suggested that HULIS emitted
242 from biomass burning can produce a high abundance of CHON compounds and S-containing
243 compounds were the dominant component for primary HULIS emitted from coal combustion
244 (Zhang et al., 2021; Song et al., 2018). The higher intensity of CHON compounds in winter in this
245 study further indicated the BB contribution. The contributions of S-containing compounds (CHOS
246 and CHONS groups) increased in winter which might be related to the polluted air masses

247 transported from the northern cities with increasing coal combustions emissions in winter (Song
248 et al., 2018). Notably, the relatively higher proportions of CHO and CHON groups in summer
249 were most probably related to the increasing biogenic emissions in summer, resulting in the
250 formation of some high molecular weight oligomers or highly oxidized organonitrates, which was
251 discussed in detail in section 3.4.1 and 3.4.2 in this study.

252 Table S1 and S2 displays the composition characteristics of atmospheric HULIS in the
253 summer and winter samples, including the relative intensity weighted average values of number,
254 molecular weight (MW_w), elemental ratios (O/C_w and H/C_w), double-bond equivalent (DBE_w),
255 aromaticity index (AI_w), and DBE/C_w . A total of 14387 and 15731 peaks were detected in the
256 summer and winter samples, respectively. The O/C and H/C ratios are commonly calculated to
257 evaluate the oxidation degree and saturation degree of the compounds, respectively (Ning et al.,
258 2022). The O/C_w values were in a range of 0.61-0.80 with an average value of 0.71 ± 0.07 for
259 summer samples and in a range of 0.59-0.67 with an average value of 0.62 ± 0.03 for winter
260 samples, respectively. The higher oxidation degree of summer samples than winter samples
261 indicated stronger secondary HULIS formation in summer. The H/C_w values were in a range of
262 1.38-1.46 with an average value of 1.42 ± 0.03 for summer samples and in a range of 1.33-1.41
263 with an average value of 1.36 ± 0.04 for winter samples, respectively. The O/C_w and H/C_w of each
264 molecular subgroup followed a changing trend of CHO < CHON < CHOS < CHONS compounds.
265 Most of the S-containing compounds had a O/C value ≥ 0.7 , suggesting the large amounts of highly
266 oxidized OSs in S-containing compounds which contained various functional groups and were
267 mainly from the photochemical oxidation of biogenic or anthropogenic volatile organic
268 compounds (VOCs) (Mutzel et al., 2015). The DBE values were calculated to describe the degree
269 of unsaturation of compounds and restricted the assigned molecular formulas with unreasonably
270 high or low number of rings or double bonds (Kroll et al., 2011). The related parameter DBE/C
271 was the double-bond equivalent of unit carbon which can reflect the condensed ring structures in
272 the compounds (Jiang et al., 2021). The higher DBE_w and DBE/C_w values of CHO and CHON
273 compounds were found in this study, indicating the higher unsaturation degree of these two groups.

274 Considering that double bonds can be formed by heteroatoms especially O atoms, whereas
275 make no contributions to the aromaticity of the compounds, AI_w was calculated to supplement the
276 DBE results (Song et al., 2018; Ning et al., 2019). AI_w can eliminate the contribution of O, N, and
277 S atoms to the C=C double bond density of molecules. The AI_w values of different compounds

278 groups in HULIS presented the changing trends: $AI_w(\text{CHONS}) > AI_w(\text{CHON}) > AI_w(\text{CHO}) >$
279 $AI_w(\text{CHOS})$ in summer and $AI_w(\text{CHON}) > AI_w(\text{CHO}) > AI_w(\text{CHONS}) > AI_w(\text{CHOS})$ in winter,
280 respectively. The formulas can be classified into three parts based on AI values proposed by
281 previous studies: aliphatic ($AI=0$), olefinic ($0 < AI \leq 0.5$) and aromatic ($AI > 0.5$) (Koch and Dittmar,
282 2006). As shown in Fig. S4 and S5, the aliphatic were the main components of S-containing
283 compounds in this study and the olefinic and aromatic were the main components of CHO and
284 CHON compounds. Furthermore, the aromatic proportion of CHO and CHON compounds
285 significantly increased in winter, suggesting the increasing anthropogenic emissions in winter.

286 3.3 Comparative analysis using Van Krevelen diagrams

287 In this study, the Van Krevelen diagrams (Fig. 3) were constructed to display the molecular
288 composition and categorical distribution of the collected samples (Noziere et al., 2015; Patriarca
289 et al., 2018; Li et al., 2022). According to the elemental ratios (O/C and H/C ratios) and AI values,
290 seven major compound classes were classified, including lipids-like species, lignins-like species,
291 proteins-like species, tannins-like species, carbohydrates-like species, condensed aromatics
292 structure, and unsaturated hydrocarbons (Table S3). The Van Krevelen diagrams showed similar
293 distributions in the 12 samples. The CHO and CHON compounds located in the lower left area
294 and the S-containing compounds located in the upper light area with higher O/C and H/C ratios,
295 indicating a higher degree of oxidation and saturation. The condensed aromatic structure mainly
296 consisted in the CHO and CHON compounds, further suggesting the influence of anthropogenic
297 emissions on the formation of CHO and CHON compounds.

298 Figure 4 presents the averaged relative contributions of the number of molecular formulas
299 from the seven categories in summer and winter samples, respectively. Lignins-like species
300 accounted for the highest proportion of CHO compounds with average contributions of 58 % and
301 61 % in summer and winter, respectively, followed by CHON compounds with average
302 contributions of 48 % and 57 % in summer and winter, respectively. Lignins are mainly composed
303 of carboxyl groups, alicyclic rings, aromatic rings, and other O-containing groups. Previous studies
304 have reported that lignin was a complex phenolic polymer which usually came from direct
305 biological emissions or combustions of biofuel (Ning et al., 2019; Boreddy et al., 2021; Sun et al.,
306 2021). Lignins pyrolysis products and other lignins derived molecules have been shown to be
307 oxidized into light absorbing BrC chromophore under certain conditions (Fleming et al., 2020).

308 Tannins-like species accounted for 21 %, 27 %, 23 %, and 30 % of CHO, CHON, CHOS, and
309 CHONS compounds, respectively in summer which were higher than those in winter with
310 contributions of 13 %, 16 %, 16 %, and 23 % to CHO, CHON, CHOS, and CHONS compounds,
311 respectively. Tannins-like species are a series of polyphenolic compounds containing hydroxyls
312 and carboxylic groups which have been widely reported in fogs, cloud water and aerosol samples,
313 attributing to highly oxidized organic compounds such as OSs or nitrooxy-OSs produced from the
314 nighttime chemistry between the biogenic VOCs with the NO₃ (Altieri et al., 2009; Bianco et al.,
315 2018; Ning et al., 2019; Altieri et al., 2008; Shen et al., 2021). Carbohydrates-like species which
316 contain monosaccharide, alditols, and anhydrosugars mainly consisted in CHONS compounds
317 which also had a relative higher proportion of 33 % in summer than that of 29 % in winter (Sun et
318 al., 2021). C₁₀H₁₆NO₇₋₉S, as monoterpene nitrooxy-OSs, showing high relative intensities, were
319 typical carbohydrates-like species detected in this study which represented biogenic secondary
320 organic aerosols (SOA) (Ning et al., 2019; Surratt et al., 2008; Wang et al., 2020). Both the higher
321 proportions of tannins-like and carbohydrates-like classes in summer indicated stronger biogenic
322 SOA formation in this study.

323 Proteins-like classes mainly consisted in CHOS compounds with average proportions of 29 %
324 and 38 % in summer and winter, respectively. Proteins contain peptide-like structures formed by
325 dehydration with different kinds of amino acids and consist of short chains of amino acid residues
326 (Bianco et al., 2018). These compounds are associated with photochemical oxidation processing
327 in aerosols, thus resulting in the significant formation of OSs from biogenic or anthropogenic
328 precursors in this study (Bigg and Leck, 2008).

329 Higher condensed aromatics were detected in winter with average proportions of 14 % in
330 CHO compounds and 8 % in CHON compounds, respectively which were 2-2.5 times of those in
331 summer. Condensed aromatics are important components of PAHs which were usually emitted
332 from incomplete combustion of fossil fuels (Ma et al., 2020). The increase of the proportion of
333 condensed aromatics in winter indicated the stronger influence of anthropogenic sources on
334 HULIS formation. The unsaturated hydrocarbons and lipids-like species showed the lowest
335 molecular number percentage of less than 1 % in this study. Previous studies have shown that the
336 lipids-like species were the main components of water insoluble organic compounds in aerosols
337 and could be attributed to monocarboxylic acids (Ning et al., 2022; Wozniak et al., 2008).

338 In summary, both the summer and winter samples were mainly composed of compounds from
339 biogenic origins (lignins-like, tannins-like, proteins-like, and carbohydrates-like species). More
340 tannins-like and carbohydrates-like species were detected in summer including large amounts of
341 highly oxidized OSs or nitrooxy-OSs, indicating biogenic SOA formation. More condensed
342 aromatic structures in CHO and CHON compounds were detected in winter, owing to increasing
343 anthropogenic emissions. It is noted that ESI ionization technology is more sensitive for the
344 identification of polar compounds. Therefore, the low polar or nonpolar compounds, such as PAHs
345 or their derivatives from fossil sources, were probably underestimated in this study (Jiang et al.,
346 2014; Lin et al., 2018).

347 3.4 Molecular composition of HULIS

348 3.4.1 Molecular characteristics of CHO compounds

349 The O/C_w and H/C_w ratios for the CHO compounds were 0.45-0.56 and 1.15-1.30 for the
350 summer samples and 0.42-0.48 and 0.90-1.02 for the winter samples (Table S1 and S2). The
351 summer samples showed higher oxidation degree and saturation degree. We firstly plotted the Van
352 Krevelen diagrams of the four molecular subgroups showing relative intensities for all the 12
353 samples and similar distributions of the high-intensity compounds were found in the 6 summer
354 samples and the 6 winter samples, respectively. Then we combined all the data in summer and
355 winter, respectively. As shown in Fig. 5a and 5d, the CHO compounds in summer with high
356 relative abundance were located at the area within $0.2 \leq O/C \leq 1.0$ and $1.0 \leq H/C \leq 1.7$, mainly
357 including lignins-like species and tannins-like species which were closely related to biogenic
358 emissions. On the contrary, the condensed aromatics showed high relative abundance in winter,
359 suggesting obviously different sources of HULIS in summer and winter. The DBE values
360 increased with the increasing of the C numbers (Fig. 5b and 5e). The high-intensity CHO
361 compounds in HULIS had DBE values between 3-7 with C numbers from 10 to 20 for summer
362 samples. In winter, the high-intensity CHO compounds had DBE values between 7-11 with C
363 numbers from 5 to 15. As mentioned above, the aromatic ($AI > 0.5$) proportion of CHO compounds
364 significantly increased in winter, the higher DBE values in winter further indicated the consists of
365 more highly unsaturated aromatic compounds which reflected the anthropogenic emissions.

366 The CHO compounds were classified according to the number of oxygen atoms to evaluate
367 the oxygen content. As shown in Fig. 5c and 5f, the high-intensity CHO compounds with 6-11
368 oxygen atom were detected in summer, such as $C_{15}H_{24}O_6$, $C_{15}H_{22}O_{10}$, $C_{18}H_{26}O_8$, and $C_{18}H_{26}O_9$,

369 these highly oxygenated organic molecules with high molecular weight have also been detected in
370 laboratory α -pinene ozonolysis SOA (Pospisilova et al., 2020). We further classified the CHO
371 compounds by different carbon atom numbers. As shown in Fig. S6, the C₁₇-C₂₂ compounds were
372 the main components of the CHO compounds, accounting for more than 50 % of the total number
373 of CHO molecular formulas in both summer and winter seasons. However, the total relative
374 intensities of the CHO compounds in summer were significantly higher than those in winter, of
375 which the C₂₃-C₂₆ and C₂₇-C₃₂ compounds were enriched in summer. These high molecular weight
376 compounds were probably oligomers formed from various biogenic precursors, such as isoprene,
377 sesquiterpene, and monoterpene (Daellenbach et al., 2019; Berndt et al., 2018). The high intensities
378 of these compounds in summer further indicated the stronger biogenic SOA formation in summer
379 compared with that in winter.

380 High-intensity CHO compounds with 4-9 oxygen atom were detected in winter (Fig. 5c) of
381 which the C₁₄H₁₀O₄ formula with a DBE value of 10 appeared the highest intensity, which was
382 probable functional PAHs and have been reported in HULIS from coal combustion smoke particles
383 (Song et al., 2019). As shown in Fig. S2 and S3, the C₁₄H₁₀O₄ formula appeared high intensity in
384 all the winter samples, providing the evidence of coal combustion emissions in winter. Some other
385 high-intensity compounds in winter, such as C₁₄H₈O₄ and C₁₄H₈O₅ both with DBE values of 11,
386 and C₁₃H₈O₂, C₁₃H₈O₅, and C₁₃H₈O₆ with DBE values of 10, might refer to hydroxyl substitutions
387 derived from anthracenedione and xanthone, respectively, which have been reported in secondary
388 wood combustion products (Bruns et al., 2015). C₁₅H₁₀O₆, C₁₅H₈O₆, and C₁₆H₁₂O₇ which had
389 DBE values of 11, 12, and 11, respectively, might be flavonoids which had flavone backbone, the
390 key structure of plant pigments, widely existing in plants in nature and could be important sources
391 of BrC chromophores in aged BBOA (Fleming et al., 2020; Lin et al., 2016; Huang et al., 2021).
392 Phenolic substances derived from phenol, guaiacol, and syringol are also widely existed in BBOA,
393 usually from the pyrolysis of lignins in wood, which also play an important role in aqueous-phase
394 SOA formation (Boreddy et al., 2021). For instance, C₁₃H₁₀O₃ and C₁₃H₁₀O₅ are guaiacol
395 derivatives, C₁₅H₁₆O₈ are syringol derivatives and C₁₈H₁₄O₆ and C₁₈H₁₄O₇ are phenol derivatives
396 (Sun et al., 2021). As shown in Fig. S7, the relative intensities of the CHO compounds mentioned
397 above produced from BB were found to have similar trends with the mass concentrations of
398 levoglucosan, which were significantly higher in W1-W3 samples, corresponding to the BB period

399 from 31 December 2017 to 1 January 2018, providing the evidence of BB influence on HULIS
400 formation in winter.

401 It is noted that the top compounds $C_9H_6O_7$ and $C_{10}H_6O_8$ were detected both in the summer
402 and winter samples (Fig. S2 and S3), which had DBE values of 7 and 8, respectively, containing
403 abundant condensed aromatic ring structures with high O numbers. Their peaks were also detected
404 in the HFO (heavy-fuel-oil)-fueled off-road engine samples reported before, suggesting the traffic
405 emission contributions to HULIS (Cui et al., 2019). This supported the radiocarbon analysis results
406 in this study and gave further information that the traffic emissions were important fossil sources
407 in both summer and winter seasons, which was also found in previous research which reported the
408 sources of HULIS based on the positive matrix factorization (PMF) model by Bao et al. (2022).

409 3.4.2 Molecular characteristics of CHON compounds

410 The O/C_w of CHON compounds in summer and winter were 0.57-0.71 and 0.52-0.56,
411 respectively, while the H/C_w were 1.20-1.32 and 1.00-1.11, respectively (Table S1 and S2).
412 Compared with the summer CHON compounds, the winter CHON compounds presented
413 significantly higher ion abundance (Fig. 6a and 6d). The most abundant CHON subgroups had
414 DBE values of 4-7 and 3-10 in summer and winter, respectively (Fig. 6b and 6e). Similar with the
415 CHO compounds, the higher DBE values of high-intensity CHON compounds in HULIS in winter
416 indicated a high prevalence of double bonds or ring structures. According to the N and O number,
417 the CHON compounds were classified into N_1O_x (N_1O_1 - N_1O_{15}) and N_2O_x (N_2O_2 - N_2O_{14}) subgroups
418 in summer and N_1O_x (N_1O_1 - N_1O_{12}) and N_2O_x (N_2O_2 - N_2O_{12}) subgroups in winter, respectively (Fig.
419 6c and 6f). NO_{8-12} and NO_{6-9} compounds were mostly enriched subgroups in summer and winter,
420 respectively. More oxygen-enriched CHON compounds containing O number above 9 were
421 detected in summer, implying the higher oxidation degree for summer samples. In addition, the
422 N_1O_x were both the major compounds represented average of $64 \pm 4 \%$ and $61 \pm 6 \%$ of the CHON
423 molecular formulas in summer and winter, respectively, indicating the presence of more single
424 nitro/amino substituents in CHON compounds in this study.

425 Among the CHON compounds, $95 \pm 1 \%$ and $86 \pm 3 \%$ CHON compounds had O/N values
426 ≥ 3 in summer and winter, respectively in this study, indicating these compounds contained large
427 amounts of oxidized nitrogen functional groups such as nitro compounds ($-NO_2$) and/or
428 organonitrates ($-ONO_2$) and excess oxygen atoms indicated the existence of other oxygen-
429 containing functional groups (Laskin et al., 2009). The organonitrates formation from NO_3

430 oxidation of biogenic or anthropogenic VOCs can affect the interactions between anthropogenic
431 and natural emissions (He et al., 2021; Shen et al., 2021; Wang et al., 2020). Organonitrates were
432 found to be important species contributing to SOA formation in the polluted urban environment,
433 which were enhanced under high NO_x level (Zheng et al., 2021). The significant higher relative
434 intensities of CHON compounds in winter indicated that the high NO_x environment in winter
435 promoted the formation of organonitrates and highlighted the importance of organonitrates for SOA
436 control in polluted environment.

437 Furthermore, we found that the increase of the relative abundance of CHON compounds in
438 winter was particularly significant in W1-W3 samples (Fig. S2 and S3), corresponding to the BB
439 episode. Phenols produced from the pyrolysis of lignins can react with NO₃ radicals in the
440 atmosphere, producing nitrophenols, which have been shown to be important BrC chromophore
441 in BBOA (Wang et al., 2017c; Lin et al., 2016; Cai et al., 2020). It was reported that the gas-phase
442 reactions of NO₃ radicals with phenolic substances took place at least 4 orders of magnitude faster
443 than those with aromatic hydrocarbon and even faster in the aqueous phase (Lin et al., 2017).
444 Among the top CHON compounds with high relative abundance in W1-W3 samples, such as
445 C₆H₄N₂O₆ and C₇H₆N₂O₆ both with a DBE value of 6, were refer to nitrophenols containing one
446 or two nitrogen-containing functional groups, which have been widely reported in aged BBOA,
447 indicating the increasing of the CHON compounds relative intensity in W1-W3 samples were
448 closely related to BB (Lin et al., 2017; Cai et al., 2020; Mohr et al., 2013; Kourtchev et al., 2016;
449 Lin et al., 2016). Some other top CHON compounds in winter samples such as C₉H₄NO₄ and
450 C₁₀H₆NO₄ with low O/C and H/C ratios most likely indicated the presence of condensed aromatic
451 structures in the compounds. The C₉H₄NO₄ compounds were most likely emitted from vehicle
452 emissions which have previously been reported (Cui et al., 2019).

453 It is worth noting that some high-intensity CHON compounds with low O/C and H/C ratios
454 were detected in summer samples in this study (Fig. 6a), which were closely related to aromatic
455 compounds from anthropogenic emissions. The top compounds with molecular formulas of
456 C₈H₅N₂O₂ and C₁₉H₁₁N₂O₄, which had O/N of 1 and 2, respectively, were both reduced N
457 compounds referring to N-heterocyclic compounds. Previously studies have found that the N-
458 heterocyclic aromatic compounds can be formed through the aldehyde–ammonia reactions (De
459 Haan et al., 2018; Zhang et al., 2022a). This indicated the important role of reduced N species (e.g.,
460 ammonium) in the formation of anthropogenic SOA in summer. Our results were consistent with

461 previous study conducted in Xi'an, China which also found formation of reduced N compounds in
462 light-absorbing aerosols through ammonia involved reactions in summer (Zeng et al., 2021).

463 3.4.3 Molecular characteristics of S-containing compounds (CHOS and CHONS compounds)

464 The O/C_w of CHOS compounds in summer and winter were 0.60-0.79 and 0.56-0.67,
465 respectively, while the H/C_w were 1.50-1.54 and 1.53-1.72, respectively. The O/C_w of CHONS
466 compounds in summer and winter were 0.82-1.01 and 0.76-0.94, respectively, while the H/C_w
467 were 1.57-1.65 and 1.58-1.66, respectively (Table S1 and S2). As shown in Fig. 7a, 7d, 8a, and 8d,
468 the high-intensity S-containing compounds in summer and winter were both located at the area
469 where $O/C > 0.5$ and $H/C > 1.5$, respectively. In addition, the relative intensity of S-containing
470 compounds increased with the O/C ratios, suggesting the S-containing compounds were highly
471 oxidized. A small number of high-intensity S-containing compounds with $O/C < 1.0$ and $H/C < 1.0$
472 were also found in winter in this study, which might be related to OSs and nitrooxy-OSs produced
473 from the oxidation of aromatic hydrocarbon. The CHOS compounds presenting high relative
474 abundance were rich in $O_{6-9}S$ and $O_{5-7}S$ groups in summer and winter, respectively, of which the
475 DBE values were all below 4. The CHONS compounds were rich in $O_{8-10}S$ and $O_{7-9}S$ groups in
476 summer and winter, respectively, of which the DBE values were all below 6 (Fig. 7b, 7e, 7c, 7f,
477 8b, 8e, 8c, and 8f). Compared with those of the CHO and CHON compounds, the DBE values of
478 S-containing compounds were significantly lower.

479 Among the S-containing compounds, more than 95 % of the CHOS, $CHON_1S$, and $CHON_2S$
480 formulas had O/S ratios greater than 4, 7, and 10, respectively, implying these compounds may
481 contain organic sulfate functional groups ($-OSO_3$) or one or two organic nitrate groups ($-ONO_2$)
482 and these compounds were more likely OSs or nitrooxy-OSs, presenting lower DBE values and
483 higher O/C and H/C ratios (Table S5 and S6) (O'Brien et al., 2014). The high-intensity CHONS
484 compounds observed in this study, such as $C_{10}H_{16}NO_{7-9}S$, $C_{10}H_{18}NO_{8-9}S$, $C_{10}H_{18}N_2O_{11}S$, and
485 $C_9H_{14}NO_{8-9}S$ could be nitrooxy-OSs derived from monoterpenes such as limonene and α -terpinene
486 of which we found the formulas in summer contained more oxygen atoms, indicating the higher
487 oxidation degree of these nitrooxy-OSs in summer (Figure S2 and S3) (Sun et al., 2021;
488 Bruggemann et al., 2020; Wang et al., 2020; Wang et al., 2018d).

489 The CHOS compounds with high intensity abundance, such as typical isoprene epoxydiols
490 (IEPOX) derived OSs with molecular formulas of $C_5H_8O_7S$ and $C_5H_{10}O_7S$ were both detected in
491 the summer and winter samples, of which the relative intensity of $C_5H_8O_7S$ were over 80 % in S1,

492 S2, S5, and S6 samples, indicating the significant isoprene SOA formation in summer (Kourtchev
493 et al., 2016; Kourtchev et al., 2013). The results were consistent with the PMF results reported by
494 Bao et al. (2022). The monoterpenes derived OSs such as $C_8H_{14}O_6S$, $C_8H_{14}O_8S$, $C_{10}H_{18}O_8$,
495 $C_{10}H_{14}O_6$, and $C_{11}H_{16}O_7$ were detected in both summer and winter samples in this study, which
496 could refer to monoterpene-OSs derived from α -pinene, α -terpinene, and limonene (Wang et al.,
497 2020). Moreover, OSs with high carbon numbers ($C \geq 14$) such as $C_{14}H_{22}O_7S$, $C_{14}H_{22}O_8S$,
498 $C_{14}H_{24}O_7S$, $C_{15}H_{26}O_7S$, $C_{15}H_{24}O_7S$, $C_{15}H_{24}O_8S$, and $C_{16}H_{28}O_7S$ were also observed in both
499 summer and winter samples. Long-chain alkanes emitted from vehicle emissions might be
500 precursors of these OSs which was consistent with the molecular structures of OSs collected in
501 urban areas affected by traffic emissions such as Shanghai, Los Angeles, and Beijing (Wang et al.,
502 2019a; Tao et al., 2014; Wang et al., 2016b). The aromatic OSs such as naphthalene derived OSs
503 with molecular formulas of $C_{10}H_{10}O_6S$, $C_{10}H_{10}O_7S$, and $C_{10}H_{12}O_7S$, 2-methylnaphthalene derived
504 OSs with molecular formulas of $C_9H_{12}O_6S$, $C_{11}H_{12}O_7S$, and $C_{11}H_{14}O_7S$, and hydroxybenzene
505 derived OSs with molecular formulas of $C_6H_6O_5S$ were also observed in this study (Qi et al., 2021;
506 Riva et al., 2015; Blair et al., 2017). Figure S8 further displays the ternary plot of the relative
507 intensities of OSs from biogenic precursors (e.g., isoprene and monoterpenes), long-chain alkanes
508 and aromatic hydrocarbon. As shown in Fig. S8, the biogenic OSs and long-chain alkanes OSs
509 formation were comparable in summer and winter, demonstrating both biogenic and anthropogenic
510 emission contributions to HULIS. The aromatic OSs presented higher relative intensities in winter,
511 further indicating the increasing anthropogenic emissions in winter. The presence of long-chain
512 alkanes derived OSs in both summer and winter seasons provided another evidence that the traffic
513 emission was one of the important fossil sources of HULIS in this study.

514 3.5 Comparison with organic compounds in source and atmospheric aerosol samples

515 The O/C and H/C ratios of water soluble HULIS in this study were compared with those of
516 water soluble organic compounds reported in source samples from BB, coal combustions, and
517 vehicle emissions (Tang et al., 2020; Song et al., 2018; Cui et al., 2019; Song et al., 2019), cloud
518 water samples (Bianco et al., 2018; Zhao et al., 2013), rainwater samples (Altieri et al., 2009), fog
519 samples (Brege et al., 2018), as well as aerosol samples collected in Beijing (Jang et al., 2020; Wu
520 et al., 2019a; Wang et al., 2018a), Tianjin (Han et al., 2022), Baoding (Sun et al., 2021), Shanghai
521 (Wang et al., 2017b), Guangzhou (Jiang et al., 2021), respectively in China, Mainz (Wang et al.,
522 2018b), Cork city (Kourtchev et al., 2014), and Bologna (Brege et al., 2018), respectively in

523 Europe, and Bakersfield (O'Brien et al., 2014) and Virginia (Willoughby et al., 2014), respectively
524 in the United States (Fig. 9). The O/C ratios were obviously higher than those detected in primary
525 BB, coal combustion, and vehicle emission samples. The H/C ratios of the CHO and CHON
526 compounds were comparable with the source samples, indicating the organics in HULIS
527 experienced atmospheric secondary process and the mixed sources of HULIS in this study. The
528 H/C ratios of the S-containing compounds were much higher than those of source samples which
529 could be attributed to the significant organosulfates formation in the atmosphere.

530 The O/C ratios reported in this study were also higher than those reported in aerosol samples
531 in urban area in China, further indicating the serious secondary pollution at Nanjing, China.
532 Among the CHO and CHON compounds, we found that the highest H/C ratio values were observed
533 in the southern city of Guangzhou, followed by those in Nanjing and Shanghai, and the lowest
534 values were observed in the northern cities such as Beijing, Tianjin, and Baoding, indicating the
535 higher unsaturation degree of the aerosol samples collected from the northern cities, which were
536 also considered as the heavy industrial region in China. The higher H/C ratios of aerosol samples
537 collected in Europe and the United States indicated the less anthropogenic emissions such as
538 industrial emissions from those areas.

539 **4. Conclusions**

540 This study focuses on the sources and molecular characteristics differences of water soluble
541 HULIS in summertime and wintertime from 2017 to 2018 at a suburb site of the YRD, China based
542 on the radiocarbon analysis and FT-ICR MS measurement with ESI ion source in negative mode.
543 The carbon isotope analysis results highlight the important fossil source contributions to HULIS
544 at the study site. A total of 14387 and 15731 peaks were detected in the summer and winter samples,
545 respectively based on the FT-ICR MS results. The assigned molecular formulas were classified
546 into CHO, CHON, CHOS, and CHONS subgroups according to their elemental compositions. The
547 Van Krevelen diagrams showed that more tannins-like and carbohydrates-like species were
548 detected in summer indicating biogenic SOA formation. Whereas more compounds containing
549 condensed aromatic structures were detected in winter which were derived from anthropogenic
550 emissions. The total relative intensity of CHO compounds in summer were significantly higher
551 than those in winter, containing lots of macromolecular oligomers derived from biogenic
552 precursors. The high-intensity CHO compounds in winter were mainly aromatic compounds such
553 as phenolic substances and flavonoids which were related to aged BBOA and oxidized PAHs most

554 probably from fossil fuel combustion. On the contrary, the total relative intensity of CHON
555 compounds significantly increased in winter, mainly composed of nitro compounds or
556 organonitrates. The enhanced formation of nitrophenols in winter indicated the BB influence. The
557 increasing organonitrates formation in winter highlighted the secondary N-containing compounds
558 formation via NO₃ radical-initiated oxidation processes. It is worth noting that the top CHON
559 compounds in summer were referring to aromatic reduced N compounds produced from the
560 aldehyde–ammonia reactions. The S-containing compounds were mainly composed of highly
561 oxidized OSs. The monoterpenes derived OSs and long-chain alkanes derived OSs were widely
562 observed in both summer and winter samples, while the aromatic OSs formation were found to be
563 more significant in winter. The presence of long-chain alkanes derived OSs supported the
564 radiocarbon results, indicating that the traffic emission was the important fossil sources at the study
565 site. The presence of aromatic secondary N-containing and S-containing compounds provided
566 evidence for the substantial contributions from anthropogenic SOA formation to fossil sources at
567 the study site. These results further verified the work reported before by Bao et al. (2022) based
568 on the PMF model which have found the significant anthropogenic SOA and fossil fuel
569 combustion contributions to HULIS in urban area in China at molecular level. In addition, strong
570 biogenic emission in summer and BB in winter were found in this study, highlighting the
571 importance of different control policies for each season in the future.

572

573 **Acknowledgments**

574 This research was financially supported by the National Natural Science Foundation of China
575 (grant no. 42192512) and the National Natural Science Foundation of China (grant no. 41977305).

576

577 **References**

578

579 Aiona, P. K., Luek, J. L., Timko, S. A., Powers, L. C., Gonsior, M., and Nizkorodov, S. A.: Effect
580 of photolysis on absorption and fluorescence spectra of light-absorbing secondary organic aerosols,
581 *Acs. Earth. Space. Chem.*, 2, 235-245, 10.1021/acsearthspacechem.7b00153, 2018.

582 Altieri, K. E., Seitzinger, S. P., Carlton, A. G., Turpin, B. J., Klein, G. C., and Marshall, A. G.:
583 Oligomers formed through in-cloud methylglyoxal reactions: Chemical composition, properties,

584 and mechanisms investigated by ultra-high resolution FT-ICR mass spectrometry, *Atmos.*
585 *Environ.*, 42, 1476-1490, 10.1016/j.atmosenv.2007.11.015, 2008.

586 Altieri, K. E., Turpin, B. J., and Seitzinger, S. P.: Oligomers, organosulfates, and nitrooxy
587 organosulfates in rainwater identified by ultra-high resolution electrospray ionization FT-ICR
588 mass spectrometry, *Atmos. Chem. Phys.*, 9, 2533–2542, www.atmos-chem-phys.net/9/2533/2009/,
589 2009.

590 Bao, M., Zhang, Y. L., Cao, F., Lin, Y. C., Hong, Y., Fan, M., Zhang, Y., Yang, X., and Xie, F.:
591 Light absorption and source apportionment of water soluble humic-like substances (HULIS) in
592 PM_{2.5} at Nanjing, China, *Environ. Res.*, 206, 112554, 10.1016/j.envres.2021.112554, 2022.

593 Berndt, T., Mender, B., Scholz, W., Fischer, L., Herrmann, H., Kulmala, M., and Hansel, A.:
594 Accretion product formation from ozonolysis and OH radical reaction of alpha-Pinene:
595 mechanistic insight and the influence of isoprene and ethylene, *Environ. Sci. Technol.*, 52, 11069-
596 11077, 10.1021/acs.est.8b02210, 2018.

597 Bianco, A., Deguillaume, L., Vaitilingom, M., Nicol, E., Baray, J. L., Chaumerliac, N., and
598 Bridoux, M.: Molecular characterization of cloud water samples collected at the Puy de Dome
599 (France) by Fourier transform ion cyclotron resonance mass spectrometry, *Environ. Sci. Technol.*,
600 52, 10275-10285, 10.1021/acs.est.8b01964, 2018.

601 Bigg, E. K., and Leck, C.: The composition of fragments of bubbles bursting at the ocean surface,
602 *J. Geophys. Res.*, 113, 10.1029/2007jd009078, 2008.

603 Blair, S. L., MacMillan, A. C., Drozd, G. T., Goldstein, A. H., Chu, R. K., Pasa-Tolic, L., Shaw,
604 J. B., Tolic, N., Lin, P., Laskin, J., Laskin, A., and Nizkorodov, S. A.: Molecular characterization
605 of organosulfur compounds in biodiesel and diesel fuel secondary organic aerosol, *Environ. Sci.*
606 *Technol.*, 51, 119-127, 10.1021/acs.est.6b03304, 2017.

607 Boreddy, S. K. R., Hegde, P., Aswini, A. R., and Aryasree, S.: Chemical characteristics, size
608 distributions, molecular composition, and brown carbon in South Asian outflow to the Indian
609 Ocean, *Earth. Space. Sci.*, 8, 10.1029/2020ea001615, 2021.

610 Brege, M., Paglione, M., Gilardoni, S., Decesari, S., Facchini, M. C., and Mazzoleni, L. R.:
611 Molecular insights on aging and aqueous-phase processing from ambient biomass burning
612 emissions-influenced Po Valley fog and aerosol, *Atmos. Chem. Phys.*, 18, 13197-13214,
613 10.5194/acp-18-13197-2018, 2018.

614 Bruggemann, M., Xu, R., Tilgner, A., Kwong, K. C., Mutzel, A., Poon, H. Y., Otto, T., Schaefer,
615 T., Poulain, L., Chan, M. N., and Herrmann, H.: Organosulfates in ambient aerosol: state of
616 knowledge and future research directions on formation, abundance, fate, and importance, *Environ.*
617 *Sci. Technol.*, 54, 3767-3782, 10.1021/acs.est.9b06751, 2020.

618 Bruns, E. A., Krapf, M., Orasche, J., Huang, Y., Zimmermann, R., Drinovec, L., Močnik, G., El-
619 Haddad, I., Slowik, J. G., Dommen, J., Baltensperger, U., and Prévôt, A. S. H.: Characterization
620 of primary and secondary wood combustion products generated under different burner loads,
621 *Atmos. Chem. Phys.*, 15, 2825-2841, 10.5194/acp-15-2825-2015, 2015.

622 Cai, J., Zeng, X., Zhi, G., Gligorovski, S., Sheng, G., Yu, Z., Wang, X., and Peng, P. a.: Molecular
623 composition and photochemical evolution of water-soluble organic carbon (WSOC) extracted
624 from field biomass burning aerosols using high-resolution mass spectrometry, *Atmos. Chem.*
625 *Phys.*, 20, 6115-6128, 10.5194/acp-20-6115-2020, 2020.

626 Cao, M., Yu, W., Chen, M., and Chen, M.: Characterization of nitrated aromatic compounds in
627 fine particles from Nanjing, China: Optical properties, source allocation, and secondary processes,
628 *Environ. Pollut.*, 316, 120650, 10.1016/j.envpol.2022.120650, 2023.

629 Chen, Q., Ikemori, F., Higo, H., Asakawa, D., and Mochida, M.: Chemical structural
630 characteristics of HULIS and other fractionated organic matter in urban aerosols: results from mass
631 spectral and FT-IR analysis, *Environ. Sci. Technol.*, 50, 1721-1730, 10.1021/acs.est.5b05277,
632 2016.

633 Chen, Y., Ge, X., Chen, H., Xie, X., Chen, Y., Wang, J., Ye, Z., Bao, M., Zhang, Y., and Chen,
634 M.: Seasonal light absorption properties of water-soluble brown carbon in atmospheric fine
635 particles in Nanjing, China, *Atmos. Environ.*, 187, 230-240, 10.1016/j.atmosenv.2018.06.002,
636 2018.

637 Chung, C. E., Ramanathan, V., and Decremier, D.: Observationally constrained estimates of
638 carbonaceous aerosol radiative forcing, *Proc. Natl. Acad. Sci. U. S. A.*, 109, 11624-11629,
639 10.1073/pnas.1203707109, 2012.

640 Cui, F., Pei, S., Chen, M., Ma, Y., and Pan, Q.: Absorption enhancement of black carbon and the
641 contribution of brown carbon to light absorption in the summer of Nanjing, China, *Atmos. Pollut.*
642 *Res.*, 12, 480-487, 10.1016/j.apr.2020.12.008, 2021.

643 Cui, M., Li, C., Chen, Y., Zhang, F., Li, J., Jiang, B., Mo, Y., Li, J., Yan, C., Zheng, M., Xie, Z.,
644 Zhang, G., and Zheng, J.: Molecular characterization of polar organic aerosol constituents in off-

645 road engine emissions using Fourier transform ion cyclotron resonance mass spectrometry (FT-
646 ICR MS): implications for source apportionment, *Atmos. Chem. Phys.*, 19, 13945-13956,
647 10.5194/acp-19-13945-2019, 2019.

648 Daellenbach, K. R., Kourtchev, I., Vogel, A. L., Bruns, E. A., Jiang, J., Petäjä, T., Jaffrezo, J.-L.,
649 Aksoyoglu, S., Kalberer, M., Baltensperger, U., El Haddad, I., and Prévôt, A. S. H.: Impact of
650 anthropogenic and biogenic sources on the seasonal variation in the molecular composition of
651 urban organic aerosols: a field and laboratory study using ultra-high-resolution mass spectrometry,
652 *Atmos. Chem. Phys.*, 19, 5973-5991, 10.5194/acp-19-5973-2019, 2019.

653 De Haan, D. O., Tapavicza, E., Riva, M., Cui, T., Surratt, J. D., Smith, A. C., Jordan, M. C.,
654 Nilakantan, S., Almodovar, M., Stewart, T. N., de Loera, A., De Haan, A. C., Cazaunau, M.,
655 Gratien, A., Pangu, E., and Doussin, J. F.: Nitrogen-containing, light-Absorbing oligomers
656 produced in aerosol particles exposed to methylglyoxal, photolysis, and cloud cycling, *Environ.*
657 *Sci. Technol.*, 52, 4061-4071, 10.1021/acs.est.7b06105, 2018.

658 Fan, X., Song, J., and Peng, P. a.: Temporal variations of the abundance and optical properties of
659 water soluble Humic-Like Substances (HULIS) in PM_{2.5} at Guangzhou, China, *Atmos. Res.*, 172-
660 173, 8-15, 10.1016/j.atmosres.2015.12.024, 2016.

661 Fleming, L. T., Lin, P., Roberts, J. M., Selimovic, V., Yokelson, R., Laskin, J., Laskin, A., and
662 Nizkorodov, S. A.: Molecular composition and photochemical lifetimes of brown carbon
663 chromophores in biomass burning organic aerosol, *Atmos. Chem. Phys.*, 20, 1105-1129,
664 10.5194/acp-20-1105-2020, 2020.

665 Gu, C., Cui, S., Ge, X., Wang, Z., Chen, M., Qian, Z., Liu, Z., Wang, X., and Zhang, Y.: Chemical
666 composition, sources and optical properties of nitrated aromatic compounds in fine particulate
667 matter during winter foggy days in Nanjing, China, *Environ. Res.*, 212, 113255,
668 10.1016/j.envres.2022.113255, 2022.

669 Glasius, M., Thomsen, D., Wang, K., Iversen, L. S., Duan, J., and Huang, R. J.: Chemical
670 characteristics and sources of organosulfates, organosulfonates, and carboxylic acids in aerosols
671 in urban Xi'an, Northwest China, *Sci. Total. Environ.*, 151187, 10.1016/j.scitotenv.2021.151187,
672 2021.

673 Graber, E. R., and Rudich, Y.: Atmospheric HULIS: How humic-like are they? A comprehensive
674 and critical review, *Atmos. Chem. Phys.*, 6, 729-753, 10.5194/acp-6-729-2006, 2006.

675 Han, H., Feng, Y., Chen, J., Xie, Q., Chen, S., Sheng, M., Zhong, S., Wei, W., Su, S., and Fu, P.:
676 Acidification impacts on the molecular composition of dissolved organic matter revealed by FT-
677 ICR MS, *Sci. Total. Environ.*, 805, 150284, 10.1016/j.scitotenv.2021.150284, 2022.

678 He, Q., Tomaz, S., Li, C., Zhu, M., Meidan, D., Riva, M., Laskin, A., Brown, S. S., George, C.,
679 Wang, X., and Rudich, Y.: Optical properties of secondary organic aerosol produced by nitrate
680 radical oxidation of biogenic volatile organic compounds, *Environ. Sci. Technol.*, 55, 2878-2889,
681 10.1021/acs.est.0c06838, 2021.

682 Huang, L., Liu, T., and Grassian, V. H.: Radical-initiated formation of aromatic organosulfates
683 and sulfonates in the aqueous phase, *Environ. Sci. Technol.*, 54, 11857-11864,
684 10.1021/acs.est.0c05644, 2020.

685 Huang, R.-J., Yang, L., Shen, J., Yuan, W., Gong, Y., Ni, H., Duan, J., Yan, J., Huang, H., You,
686 Q., and Li, Y. J.: Chromophoric fingerprinting of brown carbon from residential biomass burning,
687 *Environ. Sci. Technol. Lett.*, 9, 102-111, 10.1021/acs.estlett.1c00837, 2021.

688 Huo, Y., Guo, Z., Li, Q., Wu, D., Ding, X., Liu, A., Huang, D., Qiu, G., Wu, M., Zhao, Z., Sun,
689 H., Song, W., Li, X., Chen, Y., Wu, T., and Chen, J.: Chemical fingerprinting of HULIS in
690 particulate matters emitted from residential coal and biomass combustion, *Environ. Sci. Technol.*,
691 55, 3593-3603, 10.1021/acs.est.0c08518, 2021.

692 Jang, K. S., Choi, M., Park, M., Park, M. H., Kim, Y. H., Seo, J., Wang, Y., Hu, M., Bae, M. S.,
693 and Park, K.: Assessment of PM_{2.5}-bound nitrogen-containing organic compounds (NOCs) during
694 winter at urban sites in China and Korea, *Environ. Pollut.*, 265, 114870,
695 10.1016/j.envpol.2020.114870, 2020.

696 Jiang, B., Liang, Y., Xu, C., Zhang, J., Hu, M., and Shi, Q.: Polycyclic aromatic hydrocarbons
697 (PAHs) in ambient aerosols from Beijing: characterization of low volatile PAHs by positive-ion
698 atmospheric pressure photoionization (APPI) coupled with Fourier transform ion cyclotron
699 resonance, *Environ. Sci. Technol.*, 48, 4716-4723, 10.1021/es405295p, 2014.

700 Jiang, H., Li, J., Chen, D., Tang, J., Cheng, Z., Mo, Y., Su, T., Tian, C., Jiang, B., Liao, Y., and
701 Zhang, G.: Biomass burning organic aerosols significantly influence the light absorption properties
702 of polarity-dependent organic compounds in the Pearl River Delta Region, China, *Environ. Int.*,
703 144, 106079, 10.1016/j.envint.2020.106079, 2020.

704 Jiang, H., Li, J., Sun, R., Tian, C., Tang, J., Jiang, B., Liao, Y., Chen, C. E., and Zhang, G.:
705 Molecular dynamics and light absorption properties of atmospheric dissolved organic matter,
706 *Environ. Sci. Technol.*, **55**, 10268-10279, 10.1021/acs.est.1c01770, 2021.

707 Koch, B. P., and Dittmar, T.: From mass to structure: an aromaticity index for high-resolution
708 mass data of natural organic matter, *Rapid. Commun. Mass. Sp.*, **20**, 926-932, 10.1002/rcm.2386,
709 2006.

710 Kourtchev, I., Fuller, S., Aalto, J., Ruuskanen, T. M., McLeod, M. W., Maenhaut, W., Jones, R.,
711 Kulmala, M., and Kalberer, M.: Molecular composition of boreal forest aerosol from Hyytiälä,
712 Finland, using ultrahigh resolution mass spectrometry, *Environ. Sci. Technol.*, **47**, 4069-4079,
713 10.1021/es3051636, 2013.

714 Kourtchev, I., O'Connor, I. P., Giorio, C., Fuller, S. J., Kristensen, K., Maenhaut, W., Wenger, J.
715 C., Sodeau, J. R., Glasius, M., and Kalberer, M.: Effects of anthropogenic emissions on the
716 molecular composition of urban organic aerosols: An ultrahigh resolution mass spectrometry study,
717 *Atmos. Environ.*, **89**, 525-532, 10.1016/j.atmosenv.2014.02.051, 2014.

718 Kourtchev, I., Godoi, R. H. M., Connors, S., Levine, J. G., Archibald, A. T., Godoi, A. F. L.,
719 Paralovo, S. L., Barbosa, C. G. G., Souza, R. A. F., Manzi, A. O., Seco, R., Sjostedt, S., Park, J.-
720 H., Guenther, A., Kim, S., Smith, J., Martin, S. T., and Kalberer, M.: Molecular composition of
721 organic aerosols in central Amazonia: an ultra-high-resolution mass spectrometry study, *Atmos.*
722 *Chem. Phys.*, **16**, 11899-11913, 10.5194/acp-16-11899-2016, 2016.

723 Kroll, J. H., Donahue, N. M., Jimenez, J. L., Kessler, S. H., Canagaratna, M. R., Wilson, K. R.,
724 Altieri, K. E., Mazzoleni, L. R., Wozniak, A. S., Bluhm, H., Mysak, E. R., Smith, J. D., Kolb, C.
725 E., and Worsnop, D. R.: Carbon oxidation state as a metric for describing the chemistry of
726 atmospheric organic aerosol, *Nat. Chem.*, **3**, 133-139, 10.1038/nchem.948, 2011.

727 Kuang, B. Y., Lin, P., Huang, X. H. H., and Yu, J. Z.: Sources of humic-like substances in the
728 Pearl River Delta, China: positive matrix factorization analysis of PM_{2.5} major components and
729 source markers, *Atmos. Chem. Phys.*, **15**, 1995-2008, 10.5194/acp-15-1995-2015, 2015.

730 Laskin, A., Smith, J. S., and Laskin, J.: Molecular characterization of nitrogen-containing organic
731 compounds in biomass burning aerosols using high-resolution mass spectrometry, *Environ. Sci.*
732 *Technol.*, **43**, 3764-3771, 10.1021/es803456n, 2009.

733 Laskin, J., Laskin, A., and Nizkorodov, S. A.: Mass spectrometry analysis in atmospheric
734 chemistry, *Anal. Chem.*, **90**, 166-189, 10.1021/acs.analchem.7b04249, 2018.

735 Levin, I., and Kromer, B.: The tropospheric $^{14}\text{CO}_2$ level in mid-latitudes of the northern
736 hemisphere (1959–2003), *Radiocarbon*, 46, 1261-1272, 10.1017/s0033822200033130, 2004.

737 Levin, I., Kromer, B., and Hammer, S.: Atmospheric $\Delta^{14}\text{CO}_2$ trend in Western European
738 background air from 2000 to 2012, *Tellus. B.*, 65, 10.3402/tellusb.v65i0.20092, 2013.

739 Li, X., Han, J., Hopke, P. K., Hu, J., Shu, Q., Chang, Q., and Ying, Q.: Quantifying primary and
740 secondary humic-like substances in urban aerosol based on emission source characterization and
741 a source-oriented air quality model, *Atmos. Chem. Phys.*, 19, 2327-2341, 10.5194/acp-19-2327-
742 2019, 2019.

743 Li, X., Yu, F., Cao, J., Fu, P., Hua, X., Chen, Q., Li, J., Guan, D., Tripathee, L., Chen, Q., and
744 Wang, Y.: Chromophoric dissolved organic carbon cycle and its molecular compositions and
745 optical properties in precipitation in the Guanzhong basin, China, *Sci. Total. Environ.*, 814, 152775,
746 10.1016/j.scitotenv.2021.152775, 2022.

747 Lin, P., Rincon, A. G., Kalberer, M., and Yu, J. Z.: Elemental composition of HULIS in the Pearl
748 River Delta Region, China: results inferred from positive and negative electrospray high resolution
749 mass spectrometric data, *Environ. Sci. Technol.*, 46, 7454-7462, 10.1021/es300285d, 2012a.

750 Lin, P., Yu, J. Z., Engling, G., and Kalberer, M.: Organosulfates in humic-like substance fraction
751 isolated from aerosols at seven locations in East Asia: a study by ultra-high-resolution mass
752 spectrometry, *Environ. Sci. Technol.*, 46, 13118-13127, 10.1021/es303570v, 2012b.

753 Lin, P., Aiona, P. K., Li, Y., Shiraiwa, M., Laskin, J., Nizkorodov, S. A., and Laskin, A.: Molecular
754 characterization of brown carbon in biomass burning aerosol particles, *Environ. Sci. Technol.*, 50,
755 11815-11824, 10.1021/acs.est.6b03024, 2016.

756 Lin, P., Bluvshstein, N., Rudich, Y., Nizkorodov, S. A., Laskin, J., and Laskin, A.: Molecular
757 chemistry of atmospheric brown carbon inferred from a nationwide biomass burning event,
758 *Environ. Sci. Technol.*, 51, 11561-11570, 10.1021/acs.est.7b02276, 2017.

759 Lin, P., Fleming, L. T., Nizkorodov, S. A., Laskin, J., and Laskin, A.: Comprehensive molecular
760 characterization of atmospheric brown carbon by high resolution mass spectrometry with
761 electrospray and atmospheric pressure photoionization, *Anal. Chem.*, 90, 12493-12502,
762 10.1021/acs.analchem.8b02177, 2018.

763 Liu, X., Zhang, Y.-L., Peng, Y., Xu, L., Zhu, C., Cao, F., Zhai, X., Haque, M. M., Yang, C., Chang,
764 Y., Huang, T., Xu, Z., Bao, M., Zhang, W., Fan, M., and Lee, X.: Chemical and optical properties

765 of carbonaceous aerosols in Nanjing, eastern China: regionally transported biomass burning
766 contribution, *Atmos. Chem. Phys.*, 19, 11213-11233, 10.5194/acp-19-11213-2019, 2019.

767 Ma, L., Li, B., Liu, Y., Sun, X., Fu, D., Sun, S., Thapa, S., Geng, J., Qi, H., Zhang, A., and Tian,
768 C.: Characterization, sources and risk assessment of PM_{2.5}-bound polycyclic aromatic
769 hydrocarbons (PAHs) and nitrated PAHs (NPAHs) in Harbin, a cold city in Northern China, *J.*
770 *Clean. Prod.*, 264, 10.1016/j.jclepro.2020.121673, 2020.

771 Ma, Y., Cheng, Y., Qiu, X., Cao, G., Fang, Y., Wang, J., Zhu, T., Yu, J., and Hu, D.: Sources and
772 oxidative potential of water-soluble humic-like substances (HULIS_{WS}) in fine particulate matter
773 (PM_{2.5}) in Beijing, *Atmos. Chem. Phys.*, 18, 5607-5617, 10.5194/acp-18-5607-2018, 2018.

774 Mo, Y., Li, J., Jiang, B., Su, T., Geng, X., Liu, J., Jiang, H., Shen, C., Ding, P., Zhong, G., Cheng,
775 Z., Liao, Y., Tian, C., Chen, Y., and Zhang, G.: Sources, compositions, and optical properties of
776 humic-like substances in Beijing during the 2014 APEC summit: Results from dual carbon isotope
777 and Fourier-transform ion cyclotron resonance mass spectrometry analyses, *Environ. Pollut.*, 239,
778 322-331, 10.1016/j.envpol.2018.04.041, 2018.

779 Mohr, C., Lopez-Hilfiker, F. D., Zotter, P., Prevot, A. S., Xu, L., Ng, N. L., Herndon, S. C.,
780 Williams, L. R., Franklin, J. P., Zahniser, M. S., Worsnop, D. R., Knighton, W. B., Aiken, A. C.,
781 Gorkowski, K. J., Dubey, M. K., Allan, J. D., and Thornton, J. A.: Contribution of nitrated phenols
782 to wood burning brown carbon light absorption in Detling, United Kingdom during winter time,
783 *Environ. Sci. Technol.*, 47, 6316-6324, 10.1021/es400683v, 2013.

784 Mutzel, A., Poulain, L., Berndt, T., Iinuma, Y., Rodigast, M., Boge, O., Richters, S., Spindler, G.,
785 Sipila, M., Jokinen, T., Kulmala, M., and Herrmann, H.: Highly oxidized multifunctional organic
786 compounds observed in tropospheric particles: a field and laboratory study, *Environ. Sci. Technol.*,
787 49, 7754-7761, 10.1021/acs.est.5b00885, 2015.

788 Ning, C., Gao, Y., Zhang, H., Yu, H., Wang, L., Geng, N., Cao, R., and Chen, J.: Molecular
789 characterization of dissolved organic matters in winter atmospheric fine particulate matters (PM_{2.5})
790 from a coastal city of northeast China, *Sci. Total. Environ.*, 689, 312-321,
791 10.1016/j.scitotenv.2019.06.418, 2019.

792 Ning, C., Gao, Y., Yu, H., Zhang, H., Geng, N., Cao, R., and Chen, J.: FT-ICR mass spectrometry
793 for molecular characterization of water-insoluble organic compounds in winter atmospheric fine
794 particulate matters, *J. Environ. Sci.*, 111, 51-60, 10.1016/j.jes.2020.12.017, 2022.

795 Noziere, B., Kalberer, M., Claeys, M., Allan, J., D'Anna, B., Decesari, S., Finessi, E., Glasius, M.,
796 Grgic, I., Hamilton, J. F., Hoffmann, T., Iinuma, Y., Jaoui, M., Kahnt, A., Kampf, C. J., Kourtev,
797 I., Maenhaut, W., Marsden, N., Saarikoski, S., Schnelle-Kreis, J., Surratt, J. D., Szidat, S.,
798 Szmigielski, R., and Wisthaler, A.: The molecular identification of organic compounds in the
799 atmosphere: state of the art and challenges, *Chem. Rev.*, 115, 3919-3983, 10.1021/cr5003485,
800 2015.

801 O'Brien, R. E., Laskin, A., Laskin, J., Rubitschun, C. L., Surratt, J. D., and Goldstein, A. H.:
802 Molecular characterization of S- and N-containing organic constituents in ambient aerosols by
803 negative ion mode high-resolution Nanospray desorption electrospray ionization mass
804 spectrometry: CalNex 2010 field study, *J. Geophys. Res. -Atmos.*, 119, 10.1002/2014jd021955,
805 2014.

806 Patriarca, C., Bergquist, J., Sjoberg, P. J. R., Tranvik, L., and Hawkes, J. A.: Online HPLC-ESI-
807 HRMS method for the analysis and comparison of different dissolved organic matter samples,
808 *Environ. Sci. Technol.*, 52, 2091-2099, 10.1021/acs.est.7b04508, 2018.

809 Pospisilova, V., Lopez-Hilfiker, F. D., Bell, D. M., Haddad, I. E., Mohr, C., Huang, W., Heikkinen,
810 L., Xiao, M., Dommen, J., Prevot, A. S. H., Baltensperger, U., and Slowik, J. G.: On the fate of
811 oxygenated organic molecules in atmospheric aerosol particles, *Sci. Adv.*, 6, 2020.

812 Qi, L., Zhang, Z., Wang, X., Deng, F., Zhao, J., and Liu, H.: Molecular characterization of
813 atmospheric particulate organosulfates in a port environment using ultrahigh resolution mass
814 spectrometry: Identification of traffic emissions, *J. Hazard. Mater.*, 419, 126431,
815 10.1016/j.jhazmat.2021.126431, 2021.

816 Riva, M., Tomaz, S., Cui, T., Lin, Y.-H., Perraudin, E., Gold, A., Stone, E. A., Villenave, E., and
817 Surratt, J. D.: Evidence for an unrecognized secondary anthropogenic source of organosulfates and
818 sulfonates: gas-phase oxidation of polycyclic aromatic hydrocarbons in the presence of sulfate
819 aerosol, *Environ. Sci. Technol.*, 49, 6654-6664, 10.1021/acs.est.5b00836, 2015.

820 Shen, H., Zhao, D., Pullinen, I., Kang, S., Vereecken, L., Fuchs, H., Acir, I. H., Tillmann, R.,
821 Rohrer, F., Wildt, J., Kiendler-Scharr, A., Wahner, A., and Mentel, T. F.: Highly oxygenated
822 organic nitrates formed from NO₃ radical-initiated oxidation of beta-Pinene, *Environ. Sci.*
823 *Technol.*, 10.1021/acs.est.1c03978, 2021.

824 Siemens, K., Morales, A., He, Q., Li, C., Hettiyadura, A. P. S., Rudich, Y., and Laskin, A.:
825 Molecular analysis of secondary brown carbon produced from the photooxidation of naphthalene,
826 *Environ. Sci. Technol.*, 2022.

827 Song, J., Li, M., Jiang, B., Wei, S., Fan, X., and Peng, P.: Molecular characterization of water-
828 soluble humic like substances in smoke particles emitted from combustion of biomass materials
829 and coal using Ultrahigh-resolution electrospray ionization fourier transform ion cyclotron
830 resonance mass spectrometry, *Environ. Sci. Technol.*, 52, 2575-2585, 10.1021/acs.est.7b06126,
831 2018.

832 Song, J., Li, M., Fan, X., Zou, C., Zhu, M., Jiang, B., Yu, Z., Jia, W., Liao, Y., and Peng, P.:
833 Molecular characterization of water- and methanol-soluble organic compounds emitted from
834 residential coal combustion using Ultrahigh-resolution electrospray ionization fourier transform
835 ion cyclotron resonance mass spectrometry, *Environ. Sci. Technol.*, 53, 13607-13617,
836 10.1021/acs.est.9b04331, 2019.

837 Song, J., Li, M., Zou, C., Cao, T., Fan, X., Jiang, B., Yu, Z., Jia, W., and Peng, P.: Molecular
838 characterization of nitrogen-containing compounds in humic-like substances emitted from
839 biomass burning and coal combustion, *Environ. Sci. Technol.*, 56, 119-130,
840 10.1021/acs.est.1c04451, 2022.

841 Sun, H., Li, X., Zhu, C., Huo, Y., Zhu, Z., Wei, Y., Yao, L., Xiao, H., and Chen, J.: Molecular
842 composition and optical property of humic-like substances (HULIS) in winter-time PM_{2.5} in the
843 rural area of North China Plain, *Atmos. Environ.*, 252, 10.1016/j.atmosenv.2021.118316, 2021.

844 Surratt, J. D., Gómez-González, Y., Chan, A. W. H., Vermeylen, R., Shahgholi, M., Kleindienst,
845 T. E., Edney, E. O., Offenberg, J. H., Lewandowski, M., Jaoui, M., Maenhaut, W., Claeys, M.,
846 Flagan, R. C., and Seinfeld, J. H.: Organosulfate formation in biogenic secondary organic aerosol,
847 *J. Phys. Chem. A* 112, 8345-8378, 10.1021/jp802310p, 2008.

848 Tang, J., Li, J., Su, T., Han, Y., Mo, Y., Jiang, H., Cui, M., Jiang, B., Chen, Y., Tang, J., Song, J.,
849 Peng, P. a., and Zhang, G.: Molecular compositions and optical properties of dissolved brown
850 carbon in biomass burning, coal combustion, and vehicle emission aerosols illuminated by
851 excitation–emission matrix spectroscopy and Fourier transform ion cyclotron resonance mass
852 spectrometry analysis, *Atmos. Chem. Phys.*, 20, 2513-2532, 10.5194/acp-20-2513-2020, 2020.

853 Tao, S., Lu, X., Levac, N., Bateman, A. P., Nguyen, T. B., Bones, D. L., Nizkorodov, S. A., Laskin,
854 J., Laskin, A., and Yang, X.: Molecular characterization of organosulfates in organic aerosols from

855 Shanghai and Los Angeles urban areas by nanospray-desorption electrospray ionization high-
856 resolution mass spectrometry, *Environ. Sci. Technol.*, 48, 10993-11001, 10.1021/es5024674, 2014.

857 Tsui, W. G., and McNeill, V. F.: Modeling secondary organic aerosol production from
858 photosensitized humic-like substances (HULIS), *Environ. Sci. Technol. Lett.*, 5, 255-259,
859 10.1021/acs.estlett.8b00101, 2018.

860 Wang, J., Ge, X., Chen, Y., Shen, Y., Zhang, Q., Sun, Y., Xu, J., Ge, S., Yu, H., and Chen, M.:
861 Highly time-resolved urban aerosol characteristics during springtime in Yangtze River Delta,
862 China: insights from soot particle aerosol mass spectrometry, *Atmos. Chem. Phys.*, 16, 9109–9127,
863 <https://doi.org/10.5194/acp-16-9109-2016>, 2016a.

864 Wang, J., Nie, W., Cheng, Y., Shen, Y., Chi, X., Wang, J., Huang, X., Xie, Y., Sun, P., Xu, Z., Qi,
865 X., Su, H., and Ding, A.: Light absorption of brown carbon in eastern China based on 3-year multi-
866 wavelength aerosol optical property observations and an improved absorption Ångström exponent
867 segregation method, *Atmos. Chem. Phys.*, 18, 9061-9074, 10.5194/acp-18-9061-2018, 2018a.

868 Wang, J., Zhao, B., Wang, S., Yang, F., Xing, J., Morawska, L., Ding, A., Kulmala, M., Kerminen,
869 V.-M., Kujansuu, J., Wang, Z., Ding, D., Zhang, X., Wang, H., Tian, M., Petäjä, T., Jiang, J., and
870 Hao, J.: Particulate matter pollution over China and the effects of control policies, *Sci. Total*
871 *Environ.*, 584–585, 426–447, <https://doi.org/10.1016/j.scitotenv.2017.01.027>, 2017a.

872 Wang, K., Zhang, Y., Huang, R.-J., Cao, J., and Hoffmann, T.: UHPLC-Orbitrap mass
873 spectrometric characterization of organic aerosol from a central European city (Mainz, Germany)
874 and a Chinese megacity (Beijing), *Atmos. Environ.*, 189, 22-29, 10.1016/j.atmosenv.2018.06.036,
875 2018b.

876 Wang, K., Zhang, Y., Huang, R. J., Wang, M., Ni, H., Kampf, C. J., Cheng, Y., Bilde, M., Glasius,
877 M., and Hoffmann, T.: Molecular characterization and source identification of atmospheric
878 particulate organosulfates using ultrahigh resolution mass spectrometry, *Environ. Sci. Technol.*,
879 53, 6192-6202, 10.1021/acs.est.9b02628, 2019a.

880 Wang, X., Hayeck, N., Brüggemann, M., Yao, L., Chen, H., Zhang, C., Emmelin, C., Chen, J.,
881 George, C., and Wang, L.: Chemical characteristics of organic aerosols in Shanghai: a Study by
882 Ultrahigh-performance liquid chromatography coupled with orbitrap mass spectrometry, *J.*
883 *Geophys. Res. -Atmos.*, 122, 11,703-711,722, 10.1002/2017jd026930, 2017b.

884 Wang, X., Heald, C. L., Liu, J., Weber, R. J., Campuzano-Jost, P., Jimenez, J. L., Schwarz, J. P.,
885 and Perring, A. E.: Exploring the observational constraints on the simulation of brown carbon,
886 *Atmos. Chem. Phys.*, 18, 635-653, 10.5194/acp-18-635-2018, 2018c.

887 Wang, X. K., Rossignol, S., Ma, Y., Yao, L., Wang, M. Y., Chen, J. M., George, C., and Wang,
888 L.: Molecular characterization of atmospheric particulate organosulfates in three megacities at the
889 middle and lower reaches of the Yangtze River, *Atmos. Chem. Phys.*, 16, 2285-2298, 10.5194/acp-
890 16-2285-2016, 2016b.

891 Wang, Y., Hu, M., Lin, P., Guo, Q., Wu, Z., Li, M., Zeng, L., Song, Y., Zeng, L., Wu, Y., Guo, S.,
892 Huang, X., and He, L.: Molecular characterization of nitrogen-containing organic compounds in
893 humic-like substances emitted from straw residue burning, *Environ. Sci. Technol.*, 51, 5951-5961,
894 10.1021/acs.est.7b00248, 2017c.

895 Wang, Y., Hu, M., Guo, S., Wang, Y., Zheng, J., Yang, Y., Zhu, W., Tang, R., Li, X., Liu, Y., Le
896 Breton, M., Du, Z., Shang, D., Wu, Y., Wu, Z., Song, Y., Lou, S., Hallquist, M., and Yu, J.: The
897 secondary formation of organosulfates under interactions between biogenic emissions and
898 anthropogenic pollutants in summer in Beijing, *Atmos. Chem. Phys.*, 18, 10693-10713,
899 10.5194/acp-18-10693-2018, 2018d.

900 Wang, Y., Hu, M., Lin, P., Tan, T., Li, M., Xu, N., Zheng, J., Du, Z., Qin, Y., Wu, Y., Lu, S., Song,
901 Y., Wu, Z., Guo, S., Zeng, L., Huang, X., and He, L.: Enhancement in particulate organic nitrogen
902 and light absorption of humic-like substances over Tibetan Plateau due to long-range transported
903 biomass burning emissions, *Environ. Sci. Technol.*, 53, 14222-14232, 10.1021/acs.est.9b06152,
904 2019b.

905 Wang, Y., Hu, M., Wang, Y.-C., Li, X., Fang, X., Tang, R., Lu, S., Wu, Y., Guo, S., Wu, Z.,
906 Hallquist, M., and Yu, J. Z.: Comparative study of particulate organosulfates in contrasting
907 atmospheric environments: field evidence for the significant influence of anthropogenic sulfate
908 and NO_x, *Environ. Sci. Technol. Lett.*, 7, 787-794, 10.1021/acs.estlett.0c00550, 2020.

909 Willoughby, A. S., Wozniak, A. S., and Hatcher, P. G.: A molecular-level approach for
910 characterizing water-insoluble components of ambient organic aerosol particulates using
911 ultrahigh-resolution mass spectrometry, *Atmos. Chem. Phys.*, 14, 10299-10314, 10.5194/acp-14-
912 10299-2014, 2014.

913 Wozniak, A. S., Bauer, J. E., Sleighter, R. L., Dickhut, R. M., and Hatcher, P. G.: Technical note:
914 Molecular characterization of aerosol-derived water soluble organic carbon using ultrahigh

915 resolution electrospray ionization Fourier transform ion cyclotron resonance mass spectrometry,
916 *Atmos. Chem. Phys.*, 8, 5099–5111, www.atmos-chem-phys.net/8/5099/2008/, 2008.

917 Wu, C., Yang, J., Fu, Q., Zhu, B., Ruan, T., and Jiang, G.: Molecular characterization of water-
918 soluble organic compounds in PM_{2.5} using ultrahigh resolution mass spectrometry, *Sci. Total*
919 *Environ.*, 668, 917-924, [10.1016/j.scitotenv.2019.03.031](https://doi.org/10.1016/j.scitotenv.2019.03.031), 2019a.

920 Wu, G., Ram, K., Fu, P., Wang, W., Zhang, Y., Liu, X., Stone, E. A., Pradhan, B. B., Dangol, P.
921 M., Panday, A. K., Wan, X., Bai, Z., Kang, S., Zhang, Q., and Cong, Z.: Water-soluble brown
922 carbon in atmospheric aerosols from Godavari (Nepal), a regional representative of South Asia,
923 *Environ. Sci. Technol.*, 53, 3471-3479, [10.1021/acs.est.9b00596](https://doi.org/10.1021/acs.est.9b00596), 2019b.

924 Xu, B., Cheng, Z., Gustafsson, Ö., Kawamura, K., Jin, B., Zhu, S., Tang, T., Zhang, B., Li, J., and
925 Zhang, G.: Compound-specific radiocarbon analysis of low molecular weight dicarboxylic acids
926 in ambient aerosols using preparative gas chromatography: method development, *Environ. Sci.*
927 *Technol. Lett.*, 8, 135-141, [10.1021/acs.estlett.0c00887](https://doi.org/10.1021/acs.estlett.0c00887), 2021.

928 Xie, M., Chen, X., Hays, M. D., Lewandowski, M., Offenber, J., Kleindienst, T. E., and Holder,
929 A. L.: Light absorption of secondary organic aerosol: composition and contribution of
930 nitroaromatic compounds, *Environ. Sci. Technol.*, 51, 11607-11616, [10.1021/acs.est.7b03263](https://doi.org/10.1021/acs.est.7b03263),
931 2017.

932 Xie, X., Chen, Y., Nie, D., Liu, Y., Liu, Y., Lei, R., Zhao, X., Li, H., and Ge, X.: Light-absorbing
933 and fluorescent properties of atmospheric brown carbon: A case study in Nanjing, China,
934 *Chemosphere*, 251, 126350, [10.1016/j.chemosphere.2020.126350](https://doi.org/10.1016/j.chemosphere.2020.126350), 2020.

935 Yang, Z., Tsona, N. T., Li, J., Wang, S., Xu, L., You, B., and Du, L.: Effects of NO_x and SO₂ on
936 the secondary organic aerosol formation from the photooxidation of 1,3,5-trimethylbenzene: A
937 new source of organosulfates, *Environ. Pollut.*, 264, 114742, [10.1016/j.envpol.2020.114742](https://doi.org/10.1016/j.envpol.2020.114742), 2020.

938 Yang, Z., Tsona, N. T., George, C., and Du, L.: Nitrogen-containing compounds enhance Light
939 absorption of aromatic-derived brown carbon, *Environ. Sci. Technol.*, [10.1021/acs.est.1c08794](https://doi.org/10.1021/acs.est.1c08794),
940 2022.

941 Zeng, Y., Ning, Y., Shen, Z., Zhang, L., Zhang, T., Lei, Y., Zhang, Q., Li, G., Xu, H., Ho, S. S.
942 H., and Cao, J.: The roles of N, S, and O in molecular absorption features of brown carbon in PM_{2.5}
943 in a typical semi-arid megacity in Northwestern China, *J. Geophys. Res: Atmospheres*, 126,
944 [10.1029/2021jd034791](https://doi.org/10.1029/2021jd034791), 2021.

945 Zhang, A., Wang, Y., Zhang, Y., Weber, R. J., Song, Y., Ke, Z., and Zou, Y.: Modeling the global
946 radiative effect of brown carbon: a potentially larger heating source in the tropical free troposphere
947 than black carbon, *Atmos. Chem. Phys.*, 20, 1901-1920, 10.5194/acp-20-1901-2020, 2020a.

948 Zhang, R., Gen, M., Liang, Z., Li, Y. J., and Chan, C. K.: Photochemical reactions of glyoxal
949 during particulate ammonium nitrate photolysis: brown carbon formation, enhanced glyoxal decay,
950 and organic phase formation, *Environ. Sci. Technol.*, 56, 1605-1614, 10.1021/acs.est.1c07211,
951 2022a.

952 Zhang, T., Shen, Z., Zhang, L., Tang, Z., Zhang, Q., Chen, Q., Lei, Y., Zeng, Y., Xu, H., and Cao,
953 J.: PM_{2.5} Humic-like substances over Xi'an, China: Optical properties, chemical functional group,
954 and source identification, *Atmos. Res.*, 234, 10.1016/j.atmosres.2019.104784, 2020b.

955 Zhang, T., Shen, Z., Zeng, Y., Cheng, C., Wang, D., Zhang, Q., Lei, Y., Zhang, Y., Sun, J., Xu,
956 H., Ho, S. S. H., and Cao, J.: Light absorption properties and molecular profiles of HULIS in PM_{2.5}
957 emitted from biomass burning in traditional "Heated Kang" in Northwest China, *Sci. Total.*
958 *Environ.*, 776, 146014, 10.1016/j.scitotenv.2021.146014, 2021.

959 Zhang, T., Huang, S., Wang, D., Sun, J., Zhang, Q., Xu, H., Hang Ho, S. S., Cao, J., and Shen, Z.:
960 Seasonal and diurnal variation of PM_{2.5} HULIS over Xi'an in Northwest China: Optical properties,
961 chemical functional group, and relationship with reactive oxygen species (ROS), *Atmos. Environ.*,
962 268, 118782, <https://doi.org/10.1016/j.atmosenv.2021.118782>, 2022b.

963 Zhang, T., Shen, Z., Huang, S., Lei, Y., Zeng, Y., Sun, J., Zhang, Q., Ho, S. S. H., Xu, H., and
964 Cao, J.: Optical properties, molecular characterizations, and oxidative potentials of different
965 polarity levels of water-soluble organic matters in winter PM_{2.5} in six China's megacities, *Sci.*
966 *Total. Environ.*, 853, 158600, <https://doi.org/10.1016/j.scitotenv.2022.158600>, 2022c.

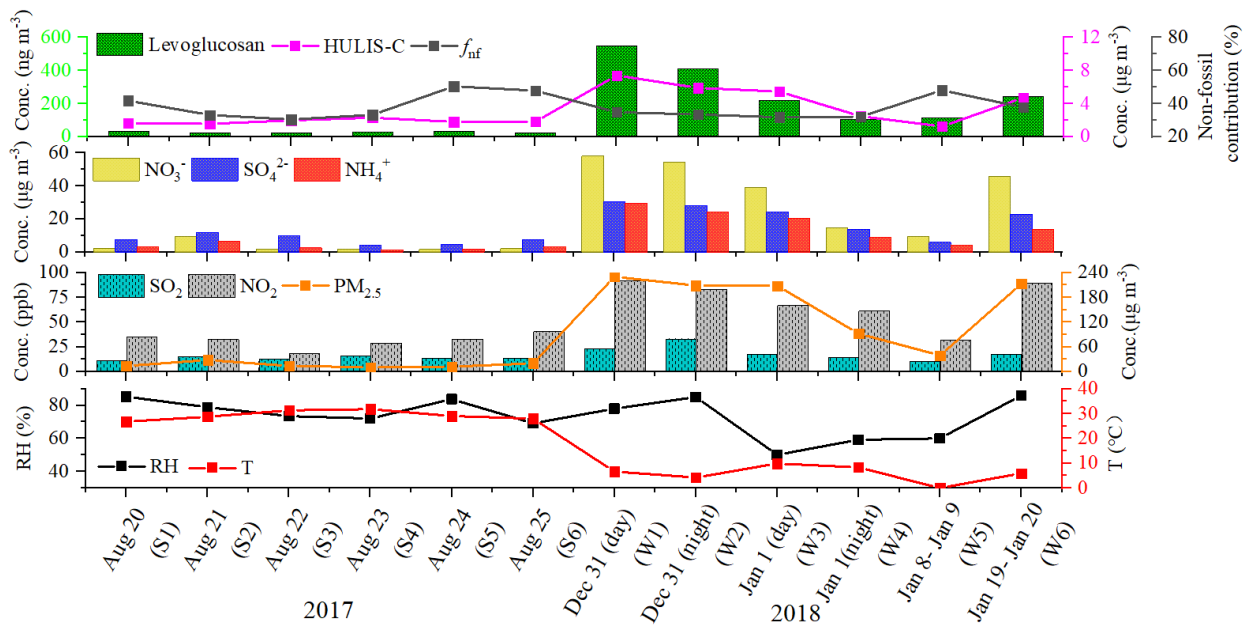
967 Zhang, Y., Forrister, H., Liu, J., Dibb, J., Anderson, B., Schwarz, J. P., Perring, A. E., Jimenez, J.
968 L., Campuzano-Jost, P., Wang, Y., Nenes, A., and Weber, R. J.: Top-of-atmosphere radiative
969 forcing affected by brown carbon in the upper troposphere, *Nat. Geosci.*, 10, 486-489,
970 10.1038/NGEO2960, 2017.

971 Zhao, M., Qiao, T., Li, Y., Tang, X., Xiu, G., and Yu, J. Z.: Temporal variations and source
972 apportionment of Hulis-C in PM_{2.5} in urban Shanghai, *Sci. Total. Environ.*, 571, 18-26,
973 10.1016/j.scitotenv.2016.07.127, 2016.

974 Zhao, Y., Hallar, A. G., and Mazzoleni, L. R.: Atmospheric organic matter in clouds: exact masses
975 and molecular formula identification using ultrahigh-resolution FT-ICR mass spectrometry,
976 *Atmos. Chem. Phys.*, 13, 12343-12362, 10.5194/acp-13-12343-2013, 2013.

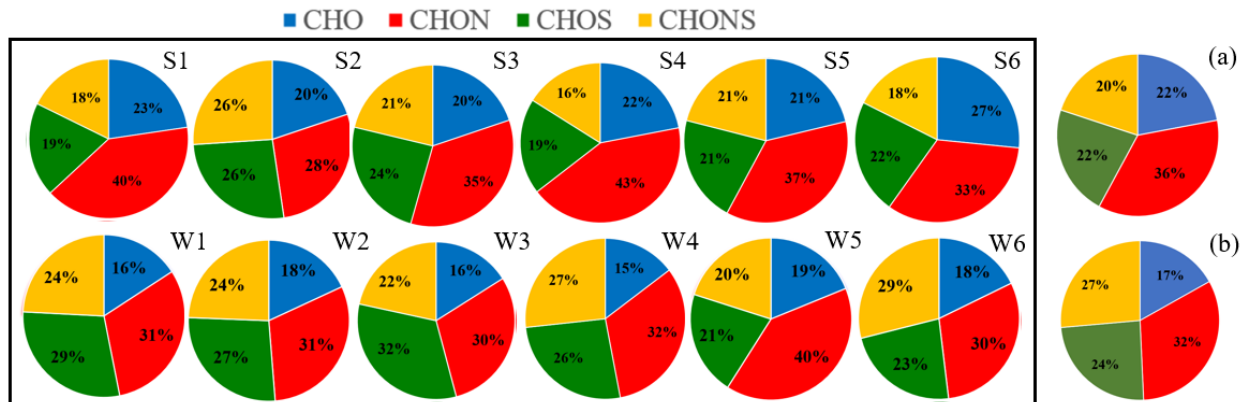
977 Zheng, G., He, K., Duan, F., Cheng, Y., and Ma, Y.: Measurement of humic-like substances in
978 aerosols: A review, *Environ. Pollut.*, 181, 301-314, 10.1016/j.envpol.2013.05.055, 2013.

979 Zheng, Y., Chen, Q., Cheng, X., Mohr, C., Cai, J., Huang, W., Shrivastava, M., Ye, P., Fu, P., Shi,
980 X., Ge, Y., Liao, K., Miao, R., Qiu, X., Koenig, T. K., and Chen, S.: Precursors and pathways
981 leading to enhanced secondary organic aerosol formation during severe haze episodes, *Environ.*
982 *Sci. Technol.*, 10.1021/acs.est.1c04255, 2021.



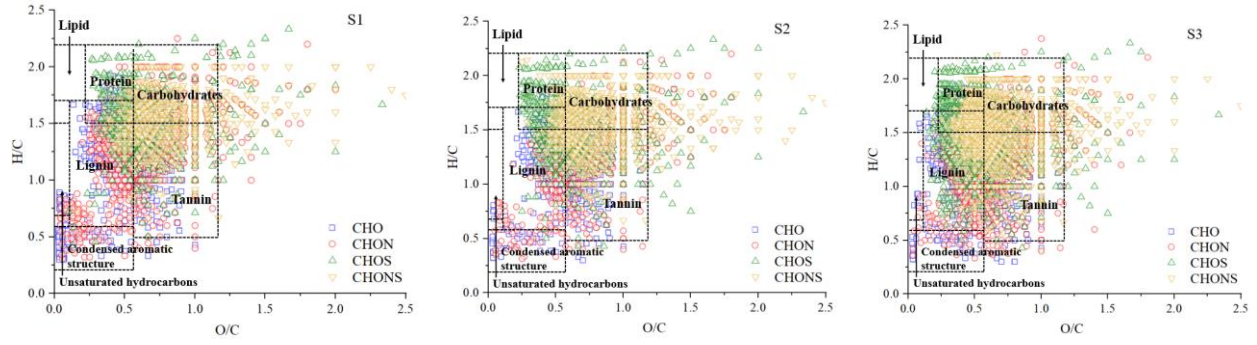
983

984 Figure 1. Time series of non-fossil contributions to HULIS-C, the mass concentrations of HULIS-
 985 C, Levoglucosan, NO_3^- , SO_4^{2-} , NH_4^+ , SO_2 , NO_2 , and $\text{PM}_{2.5}$, relative humidity, and temperature
 986 during the study periods.

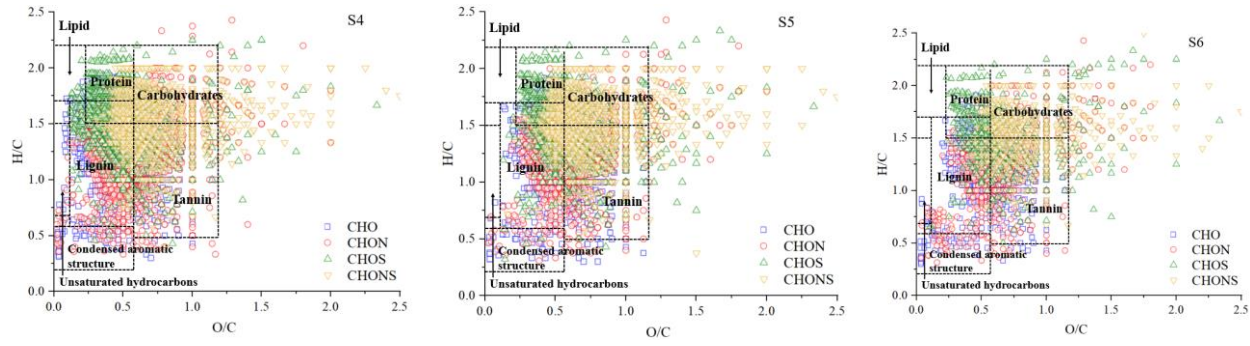


987

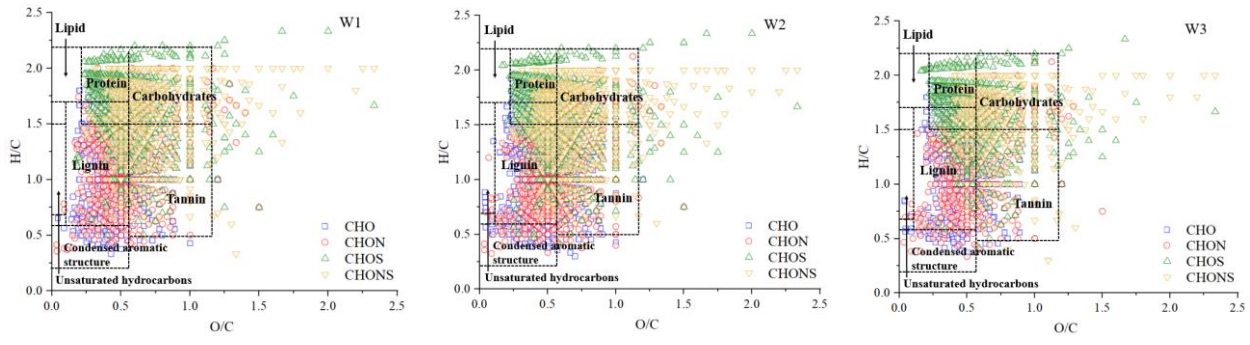
988 Figure 2. Pie graph of the number percentages of each elemental formula group for the 12 samples
 989 plotted in the box and the averaged number percentages of each elemental formula group for the
 990 summer samples (a) and winter samples (b).



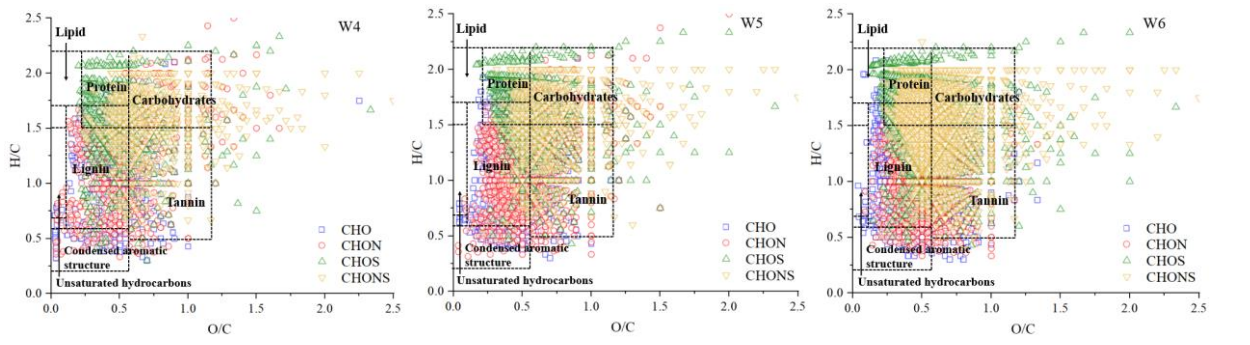
991



992



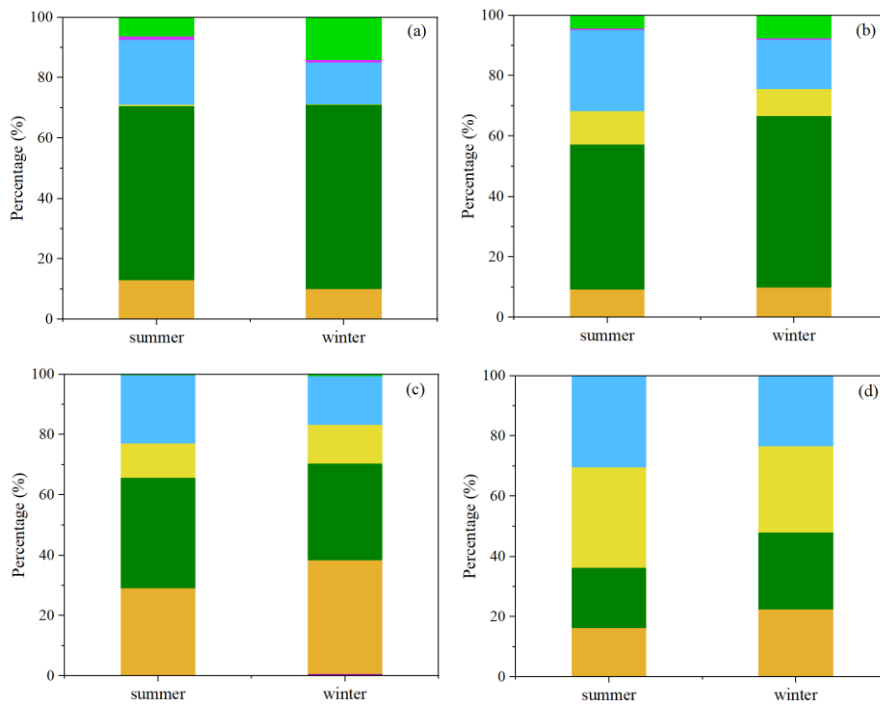
993



994

995 Figure 3. Van Krevelen diagrams of the 12 samples.

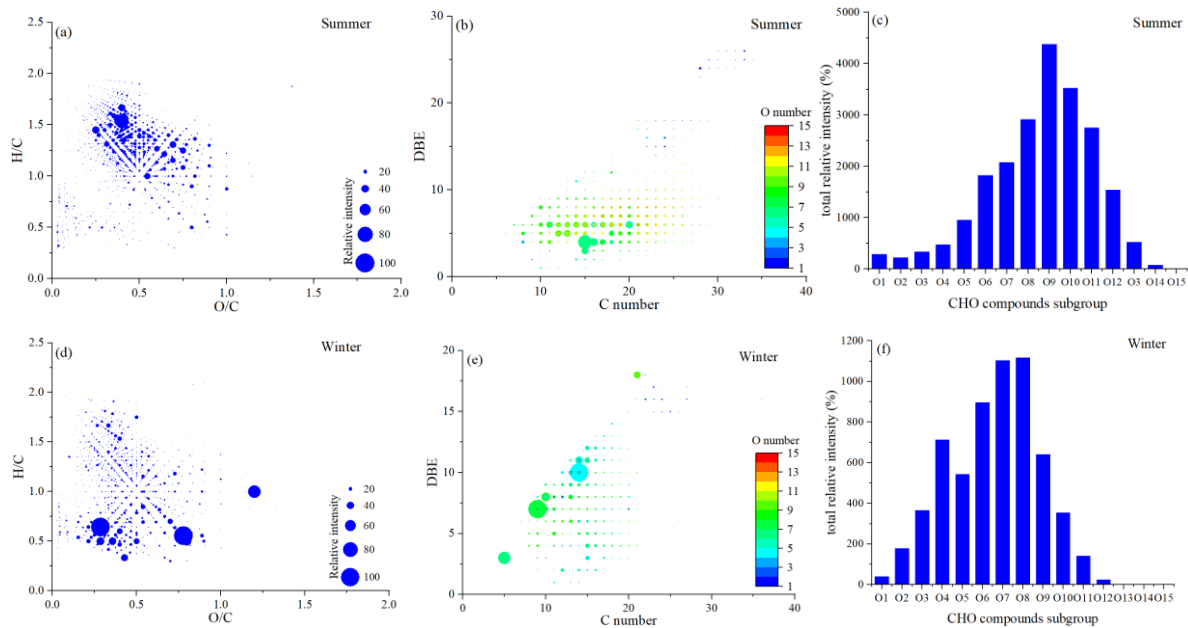
996



997

998

999 Figure 4. Contributions of seven categories in CHO (a), CHON (b), CHOS (c), and CHONS (d)
1000 compounds.

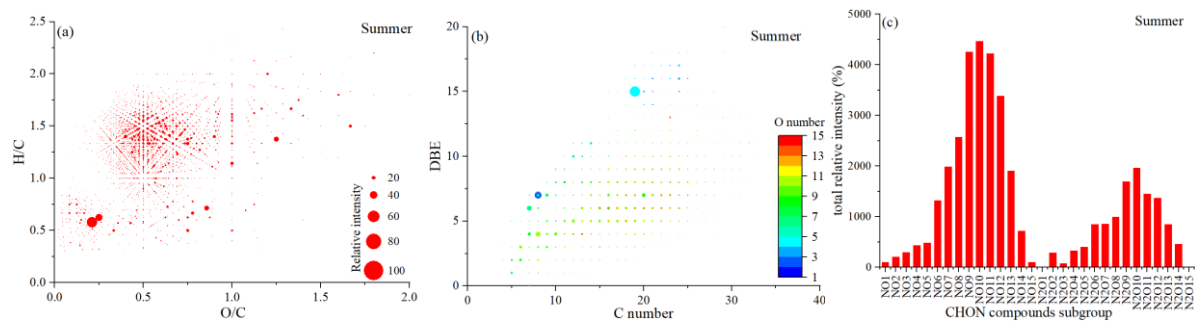


1001

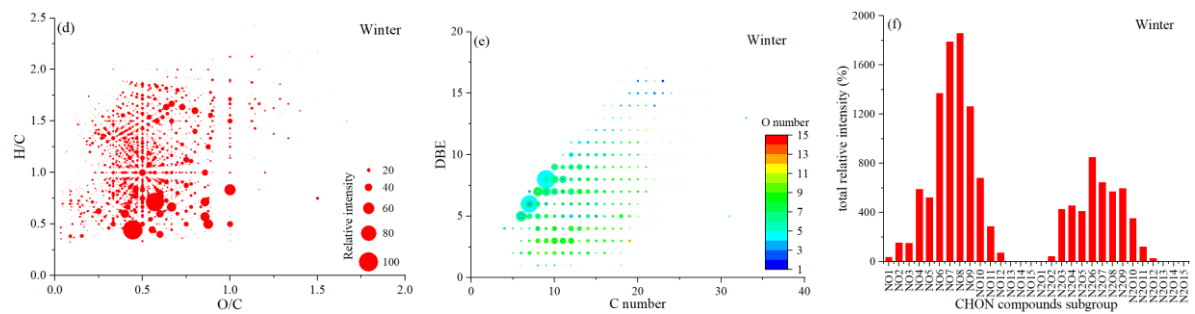
1002

1003 Figure 5. Van Krevelen diagram ((a) and (d)), plot of DBE values vs carbon atom numbers ((b)
 1004 and (e)), and the total relative intensity of each subgroup ((c) and (f)) for the CHO compounds in
 1005 summer and winter.

1006

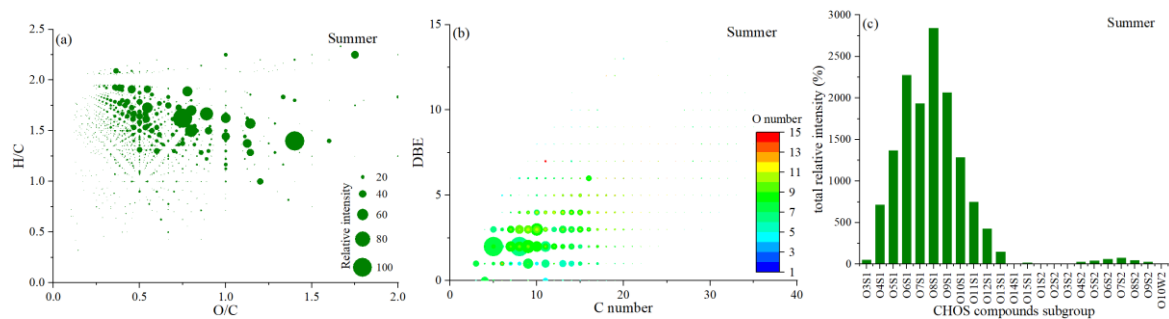


1007

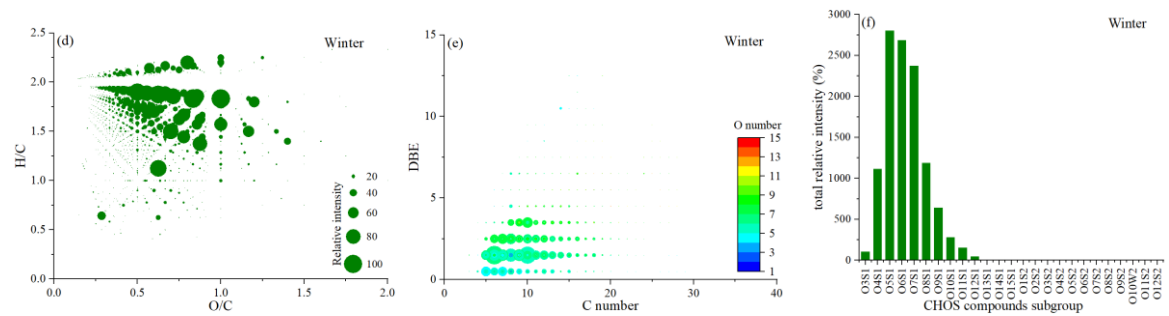


1008 Figure 6. Van Krevelen diagram ((a) and (d)), plot of DBE values vs carbon atom numbers ((b)
1009 and (e)), and the total relative intensity of each subgroup ((c) and (f)) for the CHON compounds
1010 in summer and winter.

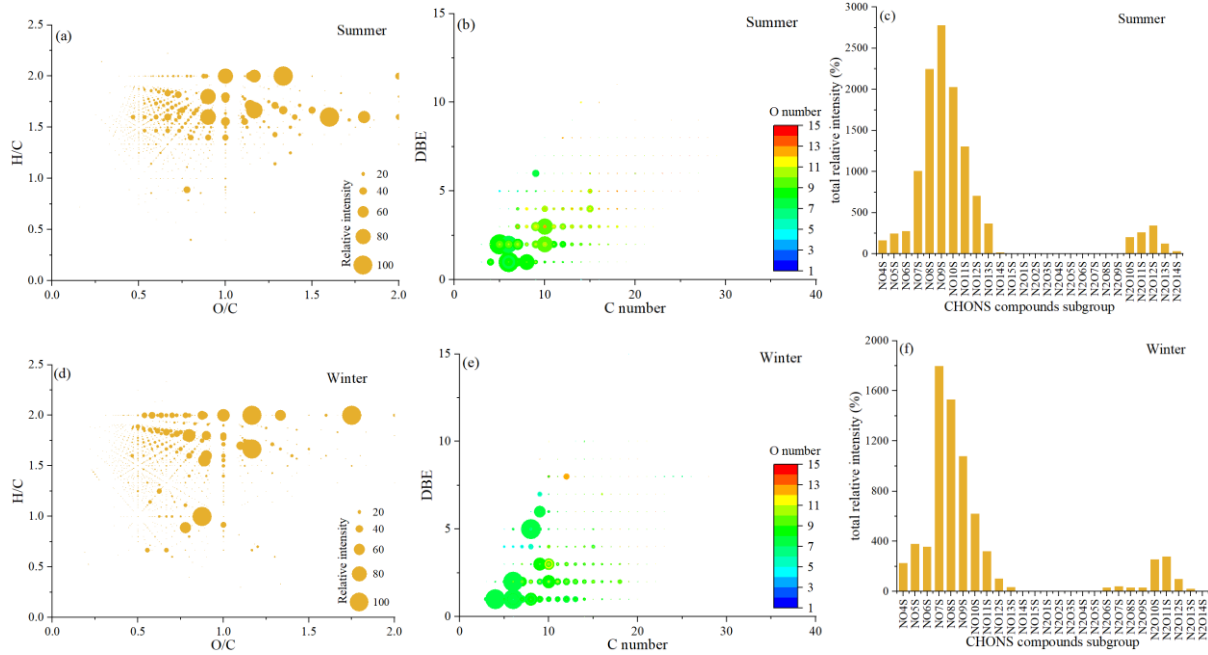
1011



1012



1013 Figure 7. Van Krevelen diagram ((a) and (d)), plot of DBE values vs carbon atom numbers ((b)
1014 and (e)), and the total relative intensity of each subgroup ((c) and (f)) for the CHOS compounds in
1015 summer and winter.

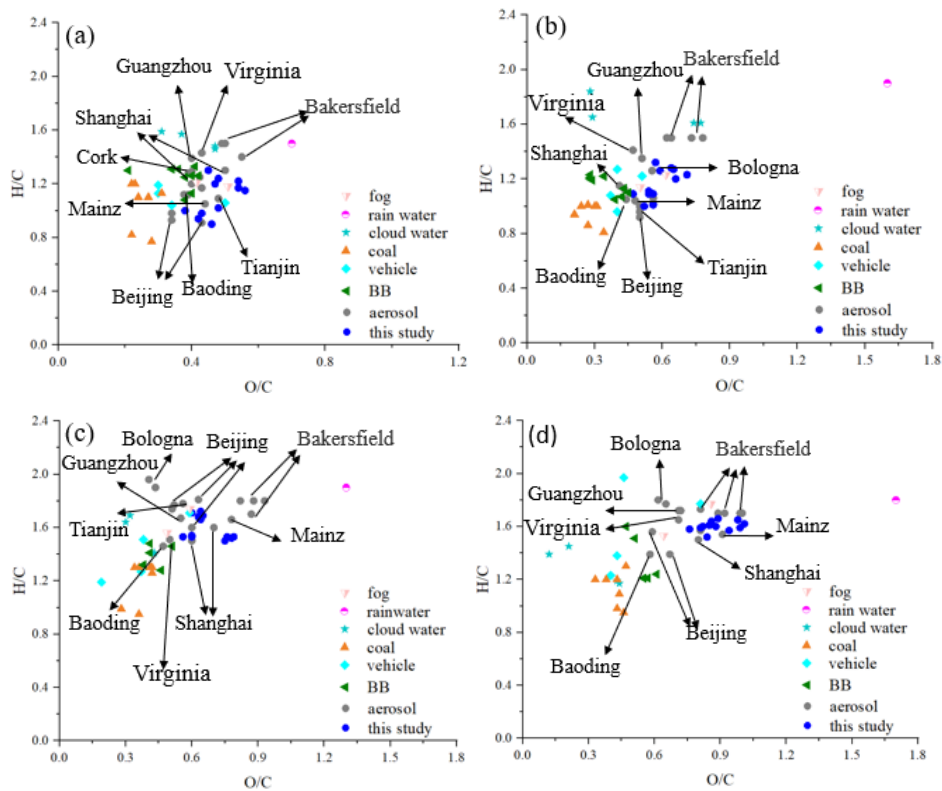


1016

1017

1018 Figure 8. Van Krevelen diagram ((a) and (d)), plot of DBE values vs carbon atom numbers ((b)
 1019 and (e)), and the total relative intensity of each subgroup ((c) and (f)) for the CHONS compounds
 1020 in summer and winter.

1021



1022

1023

1024 Figure 9. Comparison of O/C and H/C ratios of water soluble organic compounds in different
 1025 atmospheric media in CHO (a), CHON (b), CHOS (c), and CHONS (d) compounds.